J. Fluid Mech. (1976), *vol.* 74, *part* 4, *pp.* 767– 796
Printed in Great Britain

Intermittency of coherent structures in the core region of fully developed turbulent pipe flow

By JEAN SABOT AND GENEVIÈVE COMTE-BELLOT

Laboratoire de Mécanique des Fluides, Ecole Centrale de Lyon,
69130 Ecully, France

(Received 11 November 1974 and in revised form 27 November 1975)

The present investigation is oriented towards a better understanding of the turbulent structure in the core region of fully developed and completely wall-bounded flows. In view of the already existing results concerning the bursting process in boundary layers (which are semi-bounded flows), an amplitude analysis of the Reynolds shear stress fluctuation $u_1 u_2$, sorted into four quadrants of the u_1, u_2 plane, was carried out in a turbulent pipe flow. For the wall side of the core region, in which the correlation coefficient $\overline{u_1 u_2}/u_1' u_2'$ does not change appreciably with the distance from the wall, the structure of the Reynolds stress is found to be similar to that obtained in boundary layers: bursts, i.e. ejections of low speed fluid, make the dominant contribution to the Reynolds stress; the regions of violent Reynolds stress are small fractions of the overall flow; and the mean time interval between bursts is found to be almost constant across the flow. For the core region, the large cross-stream evolution of the correlation coefficient $\overline{u_1 u_2}/u_1' u_2'$ is associated with a new structure of the Reynolds stress induced by the completely wall-bounded nature of the flow. Very large amplitudes of $u_1 u_2$ are still observed, but two distinct burst-like patterns are now identified and related to ejections originating from the two opposite halves of the flow. In addition to this interaction, a focusing effect caused by the circular section of the pipe is observed. As a result of these two effects, the mean time interval between the bursts decreases significantly in the core region and reaches a minimum on the pipe axis. Investigation of specific space–time velocity correlations reveals the possible existence of rotating structures similar to those observed at the outer edge of turbulent boundary layers. These coherent motions are found to have a scale noticeably larger than that of the bursts.

1. Introduction

Much attention has to date been paid to the coherent motions present in turbulent boundary layers. 'Coherent motions' are either the bursting processes originating from the wall or the bulges moulding the free edge of the turbulent zone. The former have been extensively investigated by visual techniques (Kline, Reynolds, Schraub & Runstadler 1967; Corino & Brodkey 1969;† Kim, Kline & Reynolds 1971; Grass 1971; Nychas, Hershey & Brodkey 1973), by appropriately

† These experiments were, in effect, made in the wall region of pipe or channel flow.

processed turbulent hot-wire signals (Rao, Narasimha & Badri Narayanan 1971; Laufer & Badri Narayan 1971) or conditional sampling techniques (Wallace, Eckelmann & Brodkey 1972;† Willmarth & Lu 1972; Lu & Willmarth 1973; Brodkey, Wallace & Eckelmann 1974).† The term 'bursting' was first used by Kline *et al.* (1967) to designate a sequence of events related to the production of turbulence. The dominant features of this intermittent bursting process, which has since been extensively studied, are (i) the outward ejection of low speed fluid, briefly called 'burst', for which the instantaneous Reynolds stress $u_1 u_2(t)$ is very large and negative with $u_1 < 0$ and $u_2 > 0$ (u_1 is the fluctuating streamwise velocity and u_2 the fluctuating velocity normal to the wall), (ii) inward rushes of fluid, referred to as 'sweeps', for which $u_1 u_2(t)$ is lower than in bursts, but still relatively large and negative, with $u_1 > 0$ and $u_2 < 0$. Burst or sweep occurrence is associated with a characteristic behaviour of the fluctuating streamwise velocity at the outer edge of the viscous sublayer (i.e. at $x_2^+ \simeq 16$, where $x_2^+ \equiv x_2 U_f/\nu$ is the distance from the wall normalized with the wall-region variables; U_f is the friction velocity and ν the kinematic viscosity). When the fluctuating streamwise velocity is low and decreasing a burst occurs, whereas when it is high and increasing a sweep occurs. According to the visual observations of Grass (1971), the most violent bursts may develop across the whole boundary layer at the very low Reynolds number investigated ($Re_\theta \equiv U_\infty \theta/\nu \simeq 600$, where U_∞ is the external mean velocity and θ the momentum thickness of the boundary layer). The results obtained on the structure of the Reynolds shear stress from sampled and sorted hot-wire measurements have led Lu & Willmarth (1973) to speculate that the same situation would persist at higher Reynolds numbers ($Re_\theta \simeq 4200$ and 38 000 in their experiments). However, the visual observations of Falco (1974) do not seem to confirm this extrapolation since, for instance, at $Re_\theta \simeq 1000$–1500 bursts have been observed to originate at random positions across most of the boundary layer (i.e. in x_2 position), and these bursts travel across the flow a distance approximately equal to their streamwise extent. Near the wall, the mechanism which triggers off a burst is not yet understood, although Corino & Brodkey (1969) detected that two deterministic stages precede a burst (deceleration of the fluid near the wall, $0 \lesssim x_2^+ \lesssim 30$, and occurrence from upstream of a large disturbance of accelerated fluid which normally does not enter the region $x_2^+ \lesssim 15$). Later, Nychas, Hershey & Brodkey (1973) observed that large transverse vortices occur in the outer part of the flow, owing to a Kelvin–Helmholtz instability, and suggested that these might induce conditions in the wall region that allow an ejection to occur. Estimation of the mean time interval $\overline{T}_B$ between bursts has been attempted by several authors with a view to providing a better description of the intermittent character of the bursting process. The main difficulty is in the definitive identification of bursts. Different techniques have been used to obtain the mean time interval between bursts: (*a*) visual counting of the violent motion of ejection near the wall (Kim *et al.* 1971); (*b*) definition of the time delay corresponding to the second mild maximum of the autocorrelation coefficient of the fluctuating streamwise velocity (Kim *et al.* 1971; Laufer & Badri Narayanan 1971); (*c*) study of the periods of activity noticed in a turbulent signal

† For footnote see previous page.

that has been passed through a narrow-band filter (Rao *et al.* 1971); (*d*) conditional sampling and counting of only the most violent bursts, those for which $-u_1u_2 > 4u_1'u_2'$, where $u_i' \equiv (\overline{u_i^2})^{\frac{1}{2}}$ (Lu & Willmarth 1973); (*e*) conditional sampling and counting of all the bursts irrespective of the level of u_1u_2 (Brodkey *et al.* 1974). The variety of these techniques used to estimate the mean time interval between bursts makes the comparison of the data difficult and definite conclusions impossible. However, an interesting feature brought out by these experiments is that the mean time interval between the bursts scales better with the outer parameters of the flow that with the inner variables (Rao *et al.* 1971). This result leads one to expect a strong structural connexion between outer and inner layer zones (Laufer & Badri Narayanan 1971).

On the other hand, the turbulent/non-turbulent interface is made up of individual three-dimensional 'bulges', whose motion has been extensively investigated by Kovasznay, Kibens & Blackwelder (1970) using space–time correlation, conditional averaging, and conditional sampling techniques. It appears that the normal velocity component U_2 is the key to the understanding of the motion. Inside the bulges, there is a symmetrical part of U_2, which suggests that the bulges are subjected to an outward thrust from the interior of the turbulent field, and also an antisymmetric part of U_2, which suggests that the bulge possesses an internal rotation possibly related to the velocity gradient $\partial U_1/\partial x_2$ at the level of its origin. The mean time interval $\overline{T}_b$ between the bulges depends, of course, on the distance from the wall and therefore on the intermittency factor γ. For $\gamma = 0{\cdot}5$, certain investigations (Corrsin & Kistler 1955; Kovasznay *et al.* 1970) give $U_\infty \overline{T}_b/\delta \simeq 1{\cdot}4$ when $\overline{T}_b$ is scaled with the outer parameters of the flow. This value appears to be of the same order of magnitude as $U_\infty \overline{T}_B/\delta$ (the estimates of the mean time interval between bursts give values of $U_\infty \overline{T}_B/\delta$ between roughly 3 and 8). However, the difficulty of such a comparison should be emphasized. On the one hand, as stated previously, the determination of $\overline{T}_B$ is strongly dependent on the criterion used to detect the bursts. For instance, Lu & Willmarth (1973) have only retained 'violent' bursts, those for which $-u_1u_2 \gtrsim 4u_1'u_2'$, and obtained $U_\infty \overline{T}_B/\delta \simeq 4$. With a less severe criterion $U_\infty \overline{T}_B/\delta$ would decrease. In effect, their measurements give

$$U_\infty \overline{T}_B/\delta \simeq 1{\cdot}5 \quad \text{for} \quad -u_1u_2 \gtrsim 2u_1'u_2'$$

and

$$U_\infty \overline{T}_B/\delta \simeq 0{\cdot}45 \quad \text{for} \quad -u_1u_2 \gtrsim 0.$$

On the other hand, the bulges of the free edge can be sorted according to their duration (Antonia 1972). The longest and also the least probable bulges provide, therefore, values of $U_\infty \overline{T}_b/\delta$ which are 3 to 4 times higher than the value obtained from all the bulges irrespective of their duration. In addition, Antonia (1972) noticed that these long bulges carry with them a Reynolds shear stress distribution whose peak value is located near the upstream side of the bulges and reaches, on average, 45 % of the wall shear stress. The corresponding large amplitudes of the Reynolds shear stress fluctuation are presumably those detected in the experiments of Lu & Willmarth (1973) and identified as burst-like motions in the outer part of a boundary layer.

For completely wall-bounded flows, such as pipe or channel flows, a new situation appears in the fully developed turbulent regime because these flows, unlike the boundary layer, do not contain a free interface. The core region of pipe or channel flow appears therefore as a particular region where one can expect to find effects due to the bursting processes originating from the two opposite halves of the flow in the channel flow case, or from various azimuthal sectors in the pipe flow case. Recently, Brodkey *et al.* (1974) investigated a channel flow case but several aspects are not fully satisfactory. First, only the truncated $u_1 u_2$ signal is considered, sorted into four quadrants of the plane, i.e.

$$\begin{aligned}
&[u_1 u_2]_{\mathrm{I}}, && \text{for which} \quad u_1 u_2 > 0 \quad \text{and} \quad u_2 > 0,\\
&[u_1 u_2]_{\mathrm{II}}, && \text{for which} \quad u_1 u_2 < 0 \quad \text{and} \quad u_2 > 0,\\
&[u_1 u_2]_{\mathrm{III}}, && \text{for which} \quad u_1 u_2 > 0 \quad \text{and} \quad u_2 < 0,\\
&[u_1 u_2]_{\mathrm{IV}}, && \text{for which} \quad u_1 u_2 < 0 \quad \text{and} \quad u_2 < 0.
\end{aligned}$$

The $[u_1 u_2]_{\mathrm{II}}$ case is then associated with an ejection irrespective of the level of $u_1 u_2$. This technique attributes the same importance to the 'violent' bursts and to the 'smooth' bursts, so that the mean time obtained between successive bursts is therefore not representative of the dominant events which constitute the turbulent flow. Second, in the core region, no consideration is given to the possible events originating from the other half of the channel. For instance, the events $[u_1 u_2]_{\mathrm{III}}$, for which $u_1 u_2 > 0$ and $u_2 < 0$, are simply interpreted as 'wallward interactions' whereas they should also be considered as possible ejections originating from the opposite half of the flow. Also more recently, but with a practical computational objective in mind, Bradshaw, Dean & McEligot (1973) postulated a model for the core region. It consists of simple alternations between positively and negatively stressed regions. A thin intermediate region of fine-grained structure would then allow the mixing of the two opposite regions, but no physical basis is offered, and we shall see later that this model does not satisfactorily describe the reality.

The present investigation is therefore oriented towards a better understanding of the turbulent structure in the core region of bounded flows. Two tools will be used: (i) the statistical analysis of $u_1 u_2$ because it has been demonstrated that such an analysis is very efficient when looking for organized structures (Lu & Willmarth 1973; Antonia 1972) – especially large negative values of $u_1 u_2$ can be associated with specific events occurring in a boundary layer, mainly bursts for $[u_1 u_2]_{\mathrm{II}}$ and, to a lesser extent, sweeps for $[u_1 u_2]_{\mathrm{IV}}$ –; and (ii) the space–time correlation technique, which provides the lasting properties of the large structures, especially in a possibly intermittent region (Kovasznay *et al.* 1970).

2. Postulated flow model for the core region

From the previous discussion, a structural model of the flow in the core region of fully developed and completely wall-bounded turbulent flows can therefore be devised. This model is sketched in figure 1 and drawn for a channel flow rather

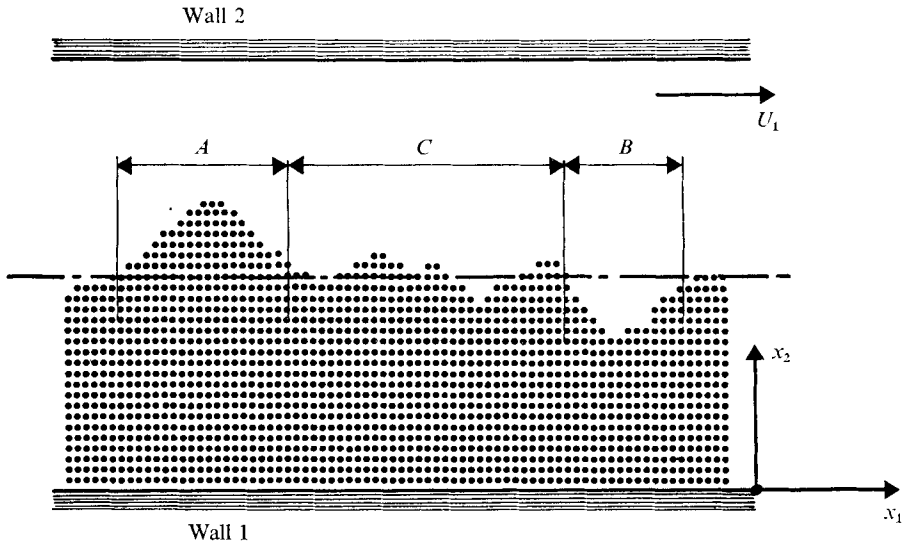

FIGURE 1. Sketch of the turbulence pattern in the core region of a plane channel. *A*, large-scale outward motion originating from the flow related to wall 1; *B*, large-scale outward motion originating from the flow related to wall 2; *C*, alternations of small-scale motions related to the opposite halves of the flow.

than a pipe flow for simplicity. It pictures large outward motions related to both halves of the flow and denoted 'bulges' as for the outer part of a boundary layer. However, it is assumed (although not apparent in the sketch) that burst-like patterns occur somewhere in the bulges on scales presumably an order of magnitude smaller than that of bulges (Antonia 1972; Falco 1974).

For such a flow model in the core region, several points have to be experimentally investigated. On the one hand, for burst-like events, the highly stressed regions related to opposite parts of the flow have to be detected (i.e. a large amplitude of $[u_1 u_2]_{\mathrm{II}}$ for bursts related to wall 1, and a large amplitude of $[u_1 u_2]_{\mathrm{III}}$ for bursts related to wall 2). In addition, the overall characteristics of bursts (mean frequency of appearance, scales, etc.) have to be compared in the core and wall region. The dependence of the spatial extent of the bursts on the Reynolds number would also be of interest. On the other hand, for bulges, a comparison has to be worked out between the characteristics of these large-scale structures as observed both in the core region of a pipe flow and in the outer part of a boundary layer. The mean spatial extent of these bulges has to be estimated and compared with those of the bursts.

3. Experimental conditions

The experiments were made in a smooth circular pipe of diameter $D = 2R = 10\,\mathrm{cm}$. All the measurements were taken at 95 diameters from the pipe inlet. The centre-line velocities were $U_{\max} \simeq 10{\cdot}2$ and $20{\cdot}3\,\mathrm{m/s}$, which gave flow Reynolds numbers $Re \equiv U_{\max} D/\nu$ of 68 000 and 135 000, hence $Re_\theta \simeq 6500$ and 12 000. The corresponding friction velocities deduced from the linear static

		Re = 135 000						Re = 68 000	
x_2/R ...	0·10	0·25	0·40	0·70	0·85	1	1·15	0·25	1
$x_2^+ = x_2U_f/\nu$	260	650	1040	1820	2210	2600	3000	350	1400
u_1'/U_f	2·30	2·00	1·70	1·00	0·87	0·78	0·87	1·90	0·79
u_2'/U_f	1·12	1·05	0·98	0·82	0·75	0·70	0·75	1·03	0·69
$L_{11}^{(1)}/R$	0·98	1·15	1·11	0·85	0·70	0·62	0·70	1·00	0·52
$L_{22}^{(1)}/R$	0·06	0·11	0·12	0·125	0·13	0·13	0·13	0·12	0·15
l/R	0·06	0·08	0·09	0·11	0·12	0·12	0·12	0·10	0·15
$U_{\max}\Theta_{11}^{(1)}/R$	12	19	19·5	15·5	11·5	7·4	11·5	15	6·5
$U_{\max}\Theta_{22}^{(1)}/R$	1·2	2·5	3·6	4·2	4·4	4·4	4·4	2·0	4·5

TABLE 1. Numerical data for the turbulence characteristics

pressure drop were respectively 0·42 m/s and 0·78 m/s. The mean velocity distribution observed in the wall region was well described by

$$U_1/U_f = 6{\cdot}05\log_{10}x_2^+ + 4{\cdot}20.$$

Statistical characteristics of the turbulence are given in table 1: r.m.s. values of u_1 and u_2; integral length scales $L_{11}^{(1)}$ and $L_{22}^{(1)}$ concerning the velocity fluctuations u_1 and u_2 and a streamwise separation r_1; integral time scales $\Theta_{11}^{(1)}$ and $\Theta_{22}^{(1)}$ of the velocity fluctuations u_1 and u_2 in a convected frame (Sabot & Comte-Bellot 1972, 1974). In the test section used, the flow can be considered as fully developed according to the available empirical criteria concerning pipe (or channel) flows, such as the lack of downstream evolution of the skewness factors $\overline{u_i^3}/(\overline{u_i^2})^{\frac{3}{2}}$ (Comte-Bellot 1965; Comte-Bellot & Marechal 1963) or the insensitivity of the u_1'/U_f profile to the entry conditions (Patel 1974; Perry & Abell 1975). The distance $x_1 = 95D$ from the inlet is also noticeably larger than the resulting length $x_m + x_r$, where x_m is the length required by the initial boundary layers to meet and x_r the length able to ensure the renewal of the turbulence (Sabot & Comte-Bellot 1972*a*, *b*, 1974). In the present conditions, $x_m \simeq x_r \simeq 35D$.

4. Amplitude analysis of the Reynolds shear stress fluctuation

4.1. *Preliminary inspection of the u_1, u_2 and u_1u_2 records*

The hot-wire equipment used to obtain the longitudinal and the radial velocity fluctuations u_1 and u_2 were Thermo Systems type 1051-2 anemometers with their linearizers, type 1055. The probe was an X-meter, DISA type 55 A 38, with 5 μm platinum wires kept at a constant overheat of 0·8. Separation of u_1 and u_2 was made by means of Burr Brown 3003-15 operational amplifiers. The product u_1u_2 was then given by a Burr Brown 4012/25 multiplier preceded by an auxiliary amplifier providing a gain adjustment. The frequency bandwidth is 2 Hz–12 kHz within -3 dB. Simultaneous traces of u_1, u_2 and u_1u_2 were obtained on a U.V. Siemens tracer type Oscilloport after recording (at 60 in./s) and playing back (at 6 in./s) the three signals by means of a Lyrec magnetic tape type TR 60.

Inspection of the traces obtained at two distances from the wall, $x_2/R = 0{\cdot}40$ and 1·0, reveals the occurrence of very large peaks of u_1u_2 for which a deter-

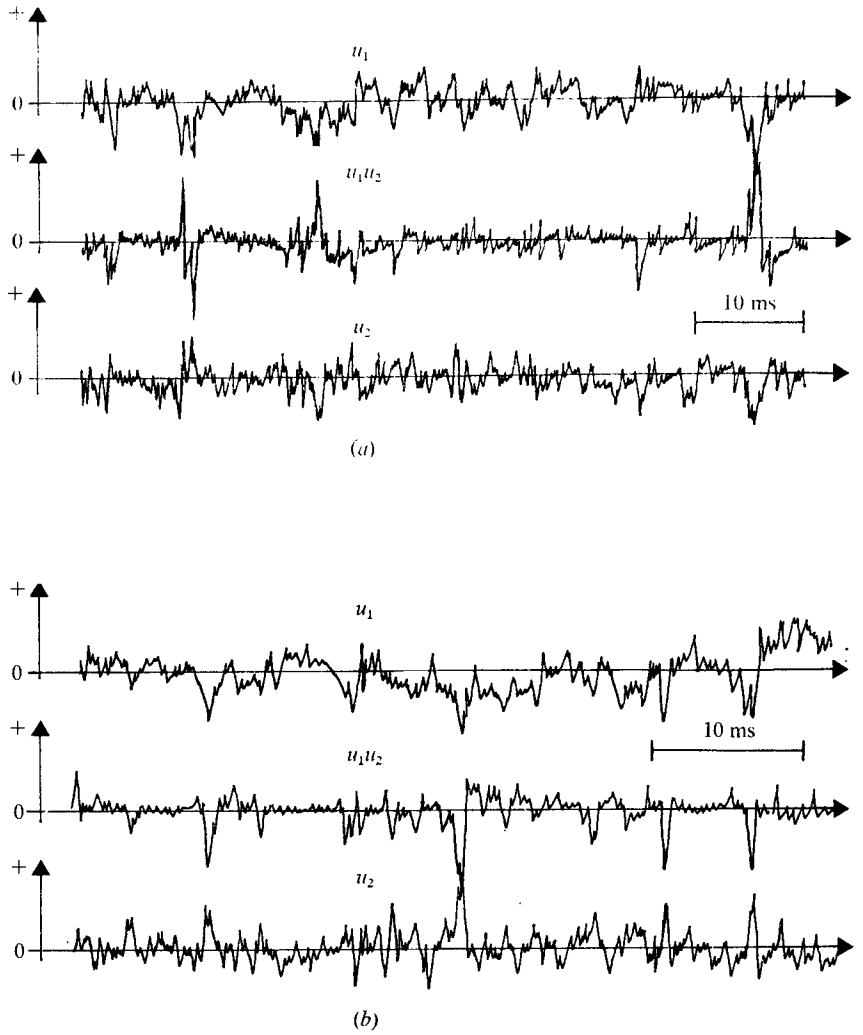

FIGURE 2. Oscillograms of velocity fluctuations u_1 and u_2 and instantaneous Reynolds shear stress u_1u_2 at $Re = 135\,000$ for two distances from the wall: (*a*) $x_2/R = 1$; (*b*) $x_2/R = 0{\cdot}40$.

ministic order prevails (figure 2). At $x_2/R = 0{\cdot}40$, the largest negative peaks of u_1u_2 appear when $u_1 < 0$ and $u_2 > 0$ and correspond to the bursts related to wall 1 (figure 1). The positive part of u_1u_2 also exhibits some large values, but the largest positive peaks have an amplitude noticeably smaller than the previous negative peaks. At $x_2/R = 1$, the negative part of u_1u_2 exhibits the same deterministic order as that observed at $x_2/R = 0{\cdot}40$, whereas the positive part of u_1u_2 has large positive peaks whose amplitudes are nearly equal to those of the large negative peaks of u_1u_2 (these observations are made over longer periods of time than those presented in figure 2). This symmetrical pattern of u_1u_2 is, of course, a consequence of the flow symmetry, which induces a zero mean value for the Reynolds stress on the axis of the pipe. In addition, most of the largest positive

peaks of $u_1 u_2$ are related to the third quadrant of the u_1, u_2 plane, i.e. to burst-like patterns related to wall 2 (figure 1).

From these preliminary inspections of the u_1, u_2 and $u_1 u_2$ records, we can conclude that (i) very large peaks of $u_1 u_2$ are detected in the core region as in the inner region, and (ii) in the core region, the mean time interval between these peaks is large and the mean duration of these peaks is short, so that the $u_1 u_2$ signal fluctuates with a relatively small amplitude over a long time. A two-state model, in which large positively and negatively stressed regions would alternate, as proposed by Bradshaw *et al.* (1973), does not appear to be a realistic description of the flow in the core region since three characteristic states are observed: two strongly stressed regions, with large positive and large negative amplitudes of $u_1 u_2$, and a weakly stressed region.

4.2. *Experimental procedure used for the amplitude analysis of the Reynolds shear stress fluctuation*

The statistical and conditional analysis of the Reynolds shear stress fluctuation used in the present experiments is somewhat similar to that used by Lu & Willmarth (1973) in a turbulent boundary layer. However, no turbulence detector was located at the edge of the viscous sublayer, so that no conditional sampling of the Reynolds shear stress was performed. For the amplitude analysis of Reynolds shear stress, the $u_1 u_2$ signal was sorted into the four quadrants of the u_1, u_2 plane. Two simultaneous conditions were therefore required to carry out the amplitude analysis in a given quadrant: the proper sign of $u_1 u_2$ and the proper sign of u_1. As long as these two conditions were not simultaneously satisfied, the $u_1 u_2$ signal was switched off (i.e. a zero voltage was running); when they were satisfied, the signal corresponding to the chosen quadrant J (J = I, II, III, IV) of the u_1, u_2 plane was recorded. After this conditional switch-off, an amplitude analysis of the resultant signal $[u_1 u_2]_J$ was performed. It consisted of counting the number of times at which the amplitude of the signal $[u_1 u_2]_J$ was equal to or greater than a given threshold: $|[u_1 u_2]_J| \geqslant |H u_1' u_2'|$. For each value of the factor H investigated, the mean frequency $\overline{N}_J$ of occurrence of the selected event was obtained, so that a frequency law $\overline{N}_J = f_J(H)$ was defined in each quadrant of the u_1, u_2 plane.

The electronic procedure used for the $u_1 u_2$ amplitude analysis is indicated in figure 3. The u_1 and $u_1 u_2$ signals were amplified by two DISA conditioners type 55 D 26. An analog gate admitted $u_1 u_2$ only when u_1 had the proper chosen sign. Its electronic block diagram is given in figure 4 and its frequency response was flat from near d.c. to 90 kHz. Another analog gate, identical to the first, generated rectangular pulses as long as the amplitude of $u_1 u_2$ remained higher than a given level. The number of pulses was then measured by a Rochar counter type A 1360 C over a 40 s period. A small overshoot occurred when $u_1 u_2$ was switched off by the first gate, so that the amplitude analysis of $u_1 u_2$ was limited towards the low level settings (for about $|u_1 u_2|/u_1' u_2' < 1{\cdot}5$).

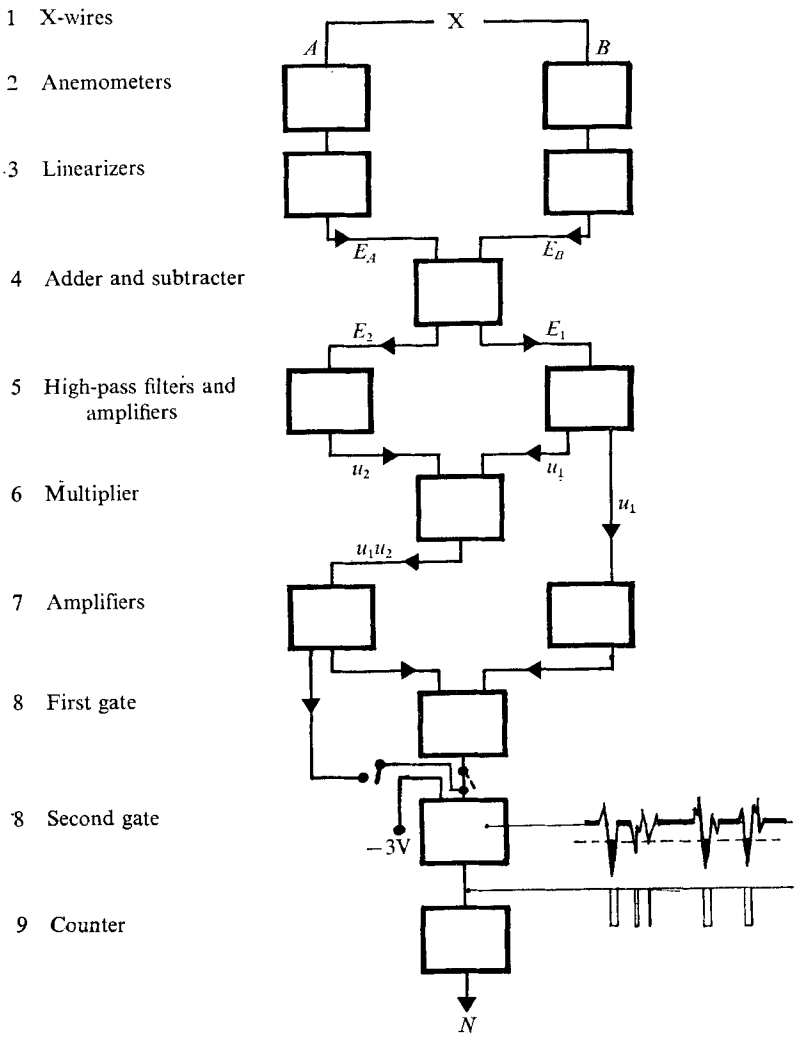

FIGURE 3. Block diagram of electronic procedure used in the u_1u_2 amplitude analysis. 1, DISA 55 A 38; 2, 3, Thermosystems Inc., Type 1051-2 and Type 1055; 4, 5, Burr Brown operational amplifier Type 3003/15; 6, Burr Brown Type 4012/25; 7, DISA conditioner Type 55 D 26; 8, analog gate (see figure 5); 9, Rochar type A 1360 C.

4.3. *Amplitude analysis of the Reynolds shear stress fluctuations in the inner region*

The term 'inner' refers to the wall side of the core region of the flow, in which the correlation coefficient $\overline{u_1u_2}/u_1'u_2'$ maintains a value nearly equal to 0·42 (i.e. for $0{\cdot}10 \lesssim x_2/R \lesssim 0{\cdot}55$, figure 5). According to the experiments of Lu & Willmarth (1973) and Brodkey *et al.* (1974), four types of motion are considered (table 2).

(i) Outward interactions, corresponding to $[u_1u_2]_{\mathrm{I}}$, for which $u_1 > 0$ and $u_2 > 0$.

(ii) Bursts, corresponding to $[u_1u_2]_{\mathrm{II}}$, for which $u_1 < 0$ and $u_2 > 0$.

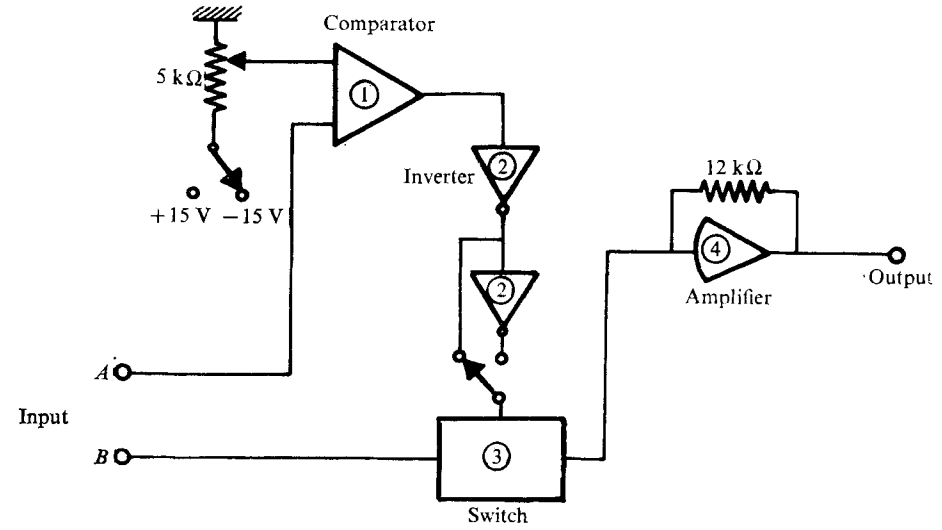

FIGURE 4. Electronic diagram of the analog gate. 1, Texas SN 72710; 2, Texas SN 7404; 3, Burr Brown 9859/15; 4, Burr Brown 3064. At the input A of the second gate either a 3 V d.c. voltage or a 100 kHz periodic pulse is applied.

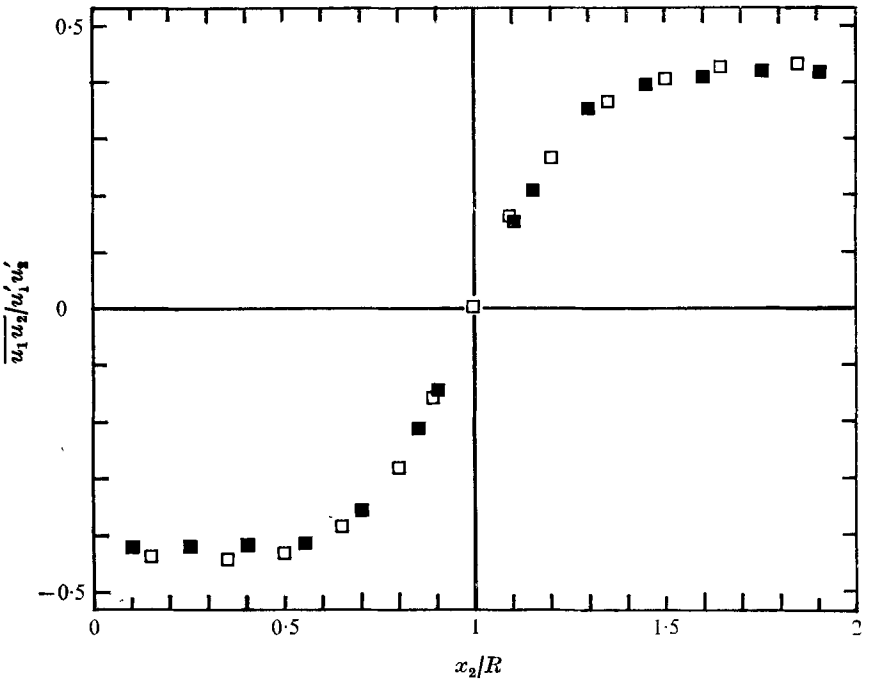

FIGURE 5. Profile of the correlation coefficient $\overline{u_1 u_2}/u_1' u_2'$ across the pipe flow. ■, Re = 68 000; □, Re = 135 000.

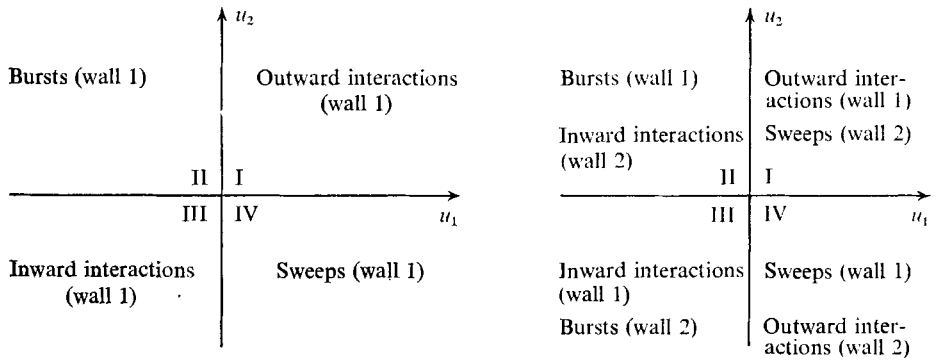

TABLE 2. Classification of the various types of events (*a*) on the wall side of the core region, (*b*) in the core region

(iii) Inward interactions, corresponding to $[u_1 u_2]_{\mathrm{III}}$, for which $u_1 < 0$ and $u_2 < 0$.

(iv) Sweeps, corresponding to $[u_1 u_2]_{\mathrm{IV}}$, for which $u_1 > 0$ and $u_2 < 0$.

In the above classification, we have assumed that the structure of the Reynolds shear stress in the inner region of wall 1 was not affected by the coherent motions initiated by the flow associated with wall 2. This assumption is based on the fact that the correlation coefficient $\overline{u_1 u_2}/u_1' u_2'$ has the same value in the inner region of a pipe flow (which is a completely wall-bounded flow) and in the inner region of a boundary layer (which is a semi-bounded flow). This similarity leads one to presume that the structures of the two flows are nearly the same.

The amplitude analysis of $u_1 u_2$ is presented in figures 6 (*a*)–(*c*) for three distances from the wall, $x_2/R = 0{\cdot}10$, $0{\cdot}25$, $0{\cdot}40$, and for $Re = 135\,000$. At each distance from the wall, the structure of the $u_1 u_2$ signal is described by the four frequency laws $\overline{N}_J = f_J(H)$ corresponding to the four quadrants of the u_1, u_2 plane (J = I, II, III, IV). In addition, the two frequency laws corresponding to the truncated $u_1 u_2$ signal [$u_1 u_2 > 0$ or $u_1 u_2 < 0$, whatever the sign of u_1] are given in figure 6. For the negative part of $u_1 u_2$ (negative values of H), very large amplitudes appear; they are ten times greater than the local value of the product $u_1' u_2'$ and twenty-five times greater than the local mean Reynolds stress $\overline{u_1 u_2}$. Bursts are therefore the dominant events in the mechanism which maintains the Reynolds shear stress, since only bursts are detected at the highest values of $|H| \equiv |u_1 u_2|/u_1' u_2'$ and since for moderate values of $|H|$ the number of bursts is noticeably higher than the number of sweeps or interactions. For the positive part of $u_1 u_2$, some large peaks are also observed, but their amplitude is lower than those of the bursts. Furthermore, it may be noticed that the frequency laws $\overline{N}_{\mathrm{I}} = f_{\mathrm{I}}(H)$ and $\overline{N}_{\mathrm{III}} = f_{\mathrm{III}}(H)$ associated with the interactions are nearly the same, whereas the frequency laws $\overline{N}_{\mathrm{II}} = f_{\mathrm{II}}(H)$ and $\overline{N}_{\mathrm{IV}} = f_{\mathrm{IV}}(H)$ for bursts and sweeps are very different.

Another general characteristic of this first set of results is the strong similarity

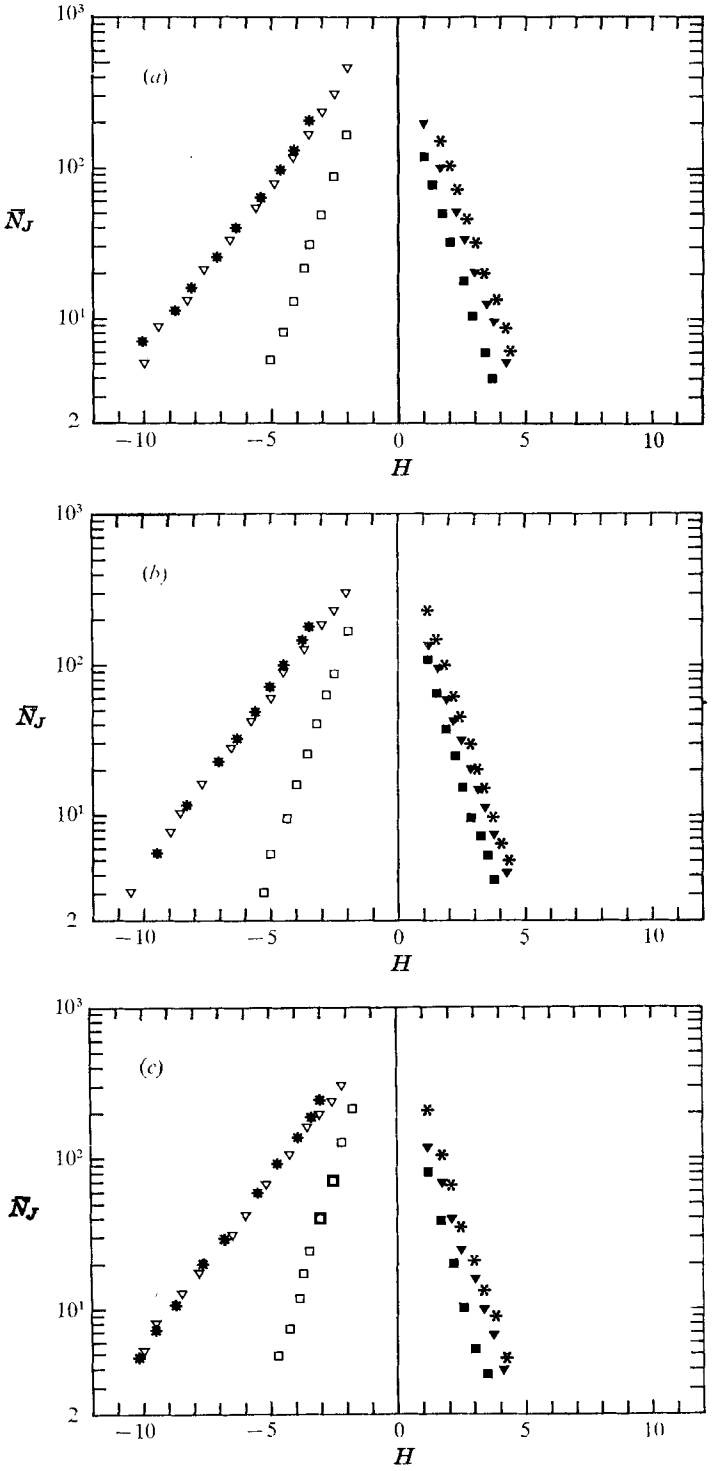

FIGURE 6. Frequency distribution of u_1u_2 as function of the threshold $H = u_1u_2/u_1'u_2'$ for the following classes of events: ✱, $u_1u_2 < 0$, whatever the sign of u_2; ✻, $u_1u_2 > 0$, whatever the sign of u_2; ■, $[u_1u_2]_{\mathrm{I}}$, outward interaction (with $u_1u_2 > 0$ and $u_2 > 0$); ▽, $[u_1u_2]_{\mathrm{II}}$, burst (with $u_1u_2 < 0$ and $u_2 > 0$); ▼, $[u_1u_2]_{\mathrm{III}}$, inward interaction (with $u_1u_2 > 0$ and $u_2 < 0$); □, $[u_1u_2]_{\mathrm{IV}}$, sweep (with $u_1u_2 < 0$ and $u_2 < 0$). $Re = 135000$. (*a*) $x_2/R = 0{\cdot}10$. (*b*) $x_2/R = 0{\cdot}25$. (*c*) $x_2/R = 0{\cdot}40$.

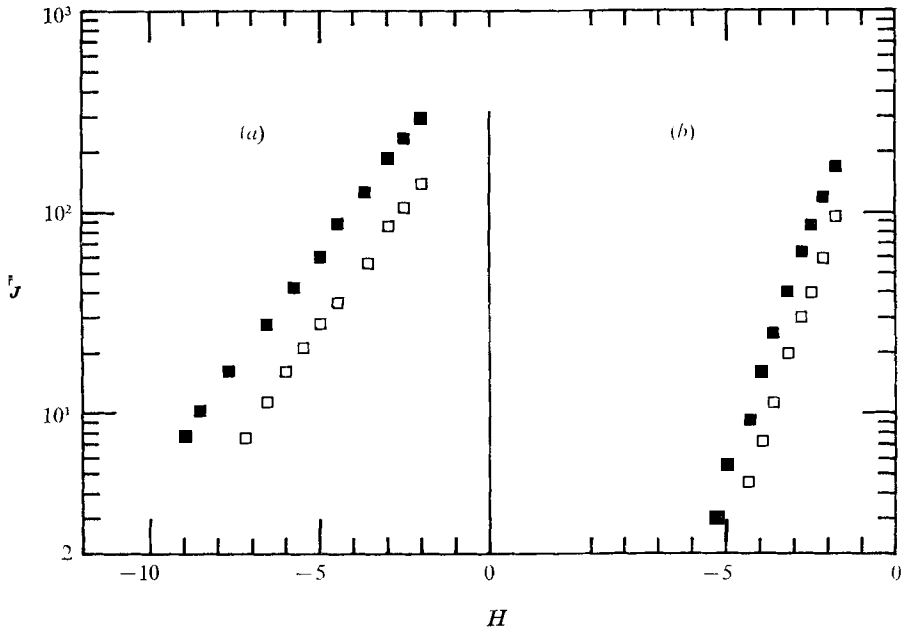

FIGURE 7. Reynolds number effect on the frequency distribution of u_1u_2. (*a*) Bursts. (*b*) Sweeps. ■, Re = 135 000; □, Re = 68 000. x_2/R = 0·25.

of every frequency law $\bar{N}_J = f_J(H)$ across the inner region, since, at given H, the mean frequency $\bar{N}_J$ does not appreciably vary with x_2/R. This property has been observed across a turbulent boundary layer (Lu & Willmarth 1973).

At the wall distance x_2/R = 0·25, the amplitude of the Reynolds shear stress fluctuation has also been analysed for Re = 68 000 and 135 000. The results are presented in figure 7 (*a*) for the bursts and figure 7 (*b*) for the sweeps. The mean frequency $\bar{N}_{\mathrm{II}}$ of occurrence of the bursts strongly depends on the Reynolds number; for a given value of H, $\bar{N}_{\mathrm{II}}$ is approximately twice as large for Re = 135 000 as for Re = 68 000. A scaling of $\bar{N}_{\mathrm{II}}$, or $\bar{T}_{\mathrm{II}} \equiv 1/\bar{N}_{\mathrm{II}}$, with the outer parameters $U_{\max}$ and R has been attempted. Figure 8 shows the distribution of $U_{\max}\bar{T}_{\mathrm{II}}/R$ *vs.* x_2/R for various values of H (H = −3, −4, −5, −6) at Re = 135 000 and Re = 68 000 (in the latter case only for x_2/R = 0·25). The mean time interval $\bar{T}_{\mathrm{II}}$ between the bursts appears to be properly scaled by the outer parameters $U_{\max}$ and R for each value of H investigated.

A comparison between the present results, which deal with the 'inner' region of a pipe flow, and the results of Lu & Willmarth (1973), which correspond to a boundary layer, is given in figure 8. In the latter case, the outer parameters are U_∞ and δ (external mean velocity and boundary-layer thickness), and the flow Reynolds number is $Re_\delta \simeq$ 48 000. The two sets of results exhibit clearly the similarity of the burst patterns in the 'inner' region of the two flows and suggest that bursts can be detected from the local structure of u_1u_2, independently of the flow conditions at the edge of the viscous layer.

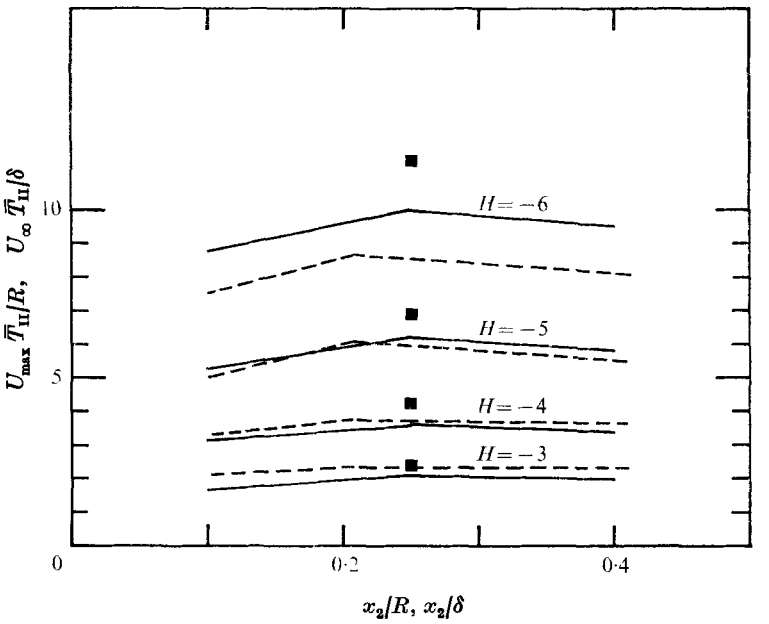

FIGURE 8. Mean time interval $\overline{T}_{II}$ between the bursts originating from a given half of the flow, as a function of the distance from the wall x_2/R and for various values of the threshold $H = u_1u_2/u_1'u_2'$. ——, pipe (Re = 135 000); ■, pipe (Re = 68 000); – – – –, boundary layer (Lu & Willmarth, Re_δ = 48 000).

4.4. *Amplitude analysis of the Reynolds shear stress fluctuation in the core region*

In the core region of the flow, the strong variation of the correlation coefficient $\overline{u_1u_2}/u_1'u_2'$ with x_2/R (figure 5) reveals a new structure of the Reynolds stress related to the completely wall-bounded nature of the flow. Because of the two opposite halves of the flow, the inventory of the classes of motions requires some modification. The possible events, related to the same co-ordinate axes as previously, are now as follows.

(i) Outward interactions corresponding to $[u_1u_2]_I$ and related as previously to the first half of the flow (wall 1) *and possibly* sweeps related to the second half of the flow (wall 2).

(ii) Bursts corresponding to $[u_1u_2]_{II}$ and related as previously to the first half of the flow, *and possibly* inward interactions related to the second half of the flow.

(iii) Inward interactions corresponding to $[u_1u_2]_{III}$ and related as previously to the first half of the flow, *and possibly* bursts related to the second half of the flow.

(iv) Sweeps corresponding to $[u_1u_2]_{II}$ and related as previously to the first half of the flow, *and possibly* outward interactions related to the second half of the flow.

A difficulty now appears for the amplitude analysis of the Reynolds shear stress fluctuation, sorted into its four quadrants of the u_1, u_2 plane, since two types of motions are *a priori* possible in every quadrant (table 2). However, the following hypotheses are reasonable: (i) the mean frequency of occurrence of every inter-

action is roughly the same across the flow; (ii) for large values of $|H|$, the mean frequency of occurrence of the interactions can be neglected compared with the mean frequency of occurrence of the bursts. These requirements are, of course, fulfilled in the 'inner' region of the pipe flow (see § 4.3). Furthermore, the results of Lu & Willmarth (1973) have shown that the contribution of the interactions to the local mean Reynolds stress remains roughly constant across a boundary layer (from about $x_2/\delta = 0{\cdot}05$ to $x_2/\delta = 0{\cdot}83$).

The results of the amplitude analysis of Reynolds shear stress fluctuation in the core region are plotted in figures 9 (*a*)–(*c*) for the largest Reynolds number investigated, $Re = 135\,000$, and for three distances from the wall, $x_2/R = 0{\cdot}70, 0{\cdot}85, 1{\cdot}0$. For the negative part of the u_1u_2 signal (negative values of H), the structure of the Reynolds stress is similar to that observed in the inner region of the flow. Very large peaks of u_1u_2 are still found in the second quadrant of the u_1, u_2 plane ($[u_1u_2]_{\mathrm{II}}$ events), and the same frequency law $\bar{N}_{\mathrm{II}} = f_{\mathrm{II}}(H)$ is approximately valid for the whole region of the flow investigated. These observations indicate the existence of bursts in the core region of the pipe flow (related to wall 1). For the positive part of the u_1u_2 signal (positive values of H) in contrast with the results obtained for the positive part of u_1u_2 in the inner region, an important dependence of the frequency laws $\bar{N}_{\mathrm{I}} = f_{\mathrm{I}}(H)$ and $\bar{N}_{\mathrm{III}} = f_{\mathrm{III}}(H)$ on x_2/R is observed for $0{\cdot}70 \lesssim x_2/R \lesssim 1$. For a given value of H, the numbers of events $\bar{N}_{\mathrm{I}}$ and $\bar{N}_{\mathrm{III}}$ increase with the distance from the wall and the two types of motions observed have clearly a burst and a sweep pattern (related to wall 2).

On the axis of the pipe, the symmetry of the flow leads to a distribution of the u_1u_2 signal symmetrical with respect to $H = 0$ (figure 9*c*). The double burst pattern observed confirms the effect of the two opposite halves of the flow noted in visual observations of the u_1, u_2 and u_1u_2 records. Taking into account this property of symmetry, some deductions can be made; for example, the amplitude analysis of the positive part of u_1u_2 at $x_2/R = 0{\cdot}85$ corresponds to the amplitude analysis which could be obtained at $x_2/R = 1{\cdot}15$ for the negative part of u_1u_2. A similar correspondence holds for the pair $x_2/R = 0{\cdot}70$ and $x_2/R = 1{\cdot}30$.

The mean time interval $\bar{T}_{\mathrm{II}}$ between bursts has been plotted in figure 10 for various values of H ($H = -2, -3, -4, -5, -6$) and for the following distances from the wall: $x_2/R = 0{\cdot}10, 0{\cdot}25, 0{\cdot}40, 0{\cdot}70, 0{\cdot}85, 1{\cdot}0, 1{\cdot}15$ ($Re = 135\,000$). These data concern only the bursts initiated in the first half of the flow (i.e. wall 1 and events of type $[u_1u_2]_{\mathrm{II}}$). For $x_2/R = 0{\cdot}85$, $1{\cdot}0$ and $1{\cdot}15$, and for $H = -2$ and -3, two sets of results have been plotted in figure 10. The first set corresponds to the values of $[u_1u_2]_{\mathrm{II}}$ directly deduced from the amplitude analysis of $[u_1u_2]_{\mathrm{II}}$, and the second set corresponds to values corrected for the inward interactions initiated by the opposite halves of the flow (§ 4.4). By symmetry, the frequency of these interactions is, at every value of H, the value observed in the 'inner' region of the pipe (frequency $\bar{N}_{\mathrm{III}}$). For each set of results and for moderate values of $|H|$, it appears that the mean time interval between the bursts is approximately constant up to $x_2/R = 0{\cdot}85$, and then strongly increases beyond the pipe axis. For $x_2/R = 1{\cdot}30$, it is difficult to identify bursts still initiated in the given half of the flow (see figure 9 (*a*); the amplitude analysis of u_1u_2 obtained at $x_2/R = 0{\cdot}70$ when $H > 0$).

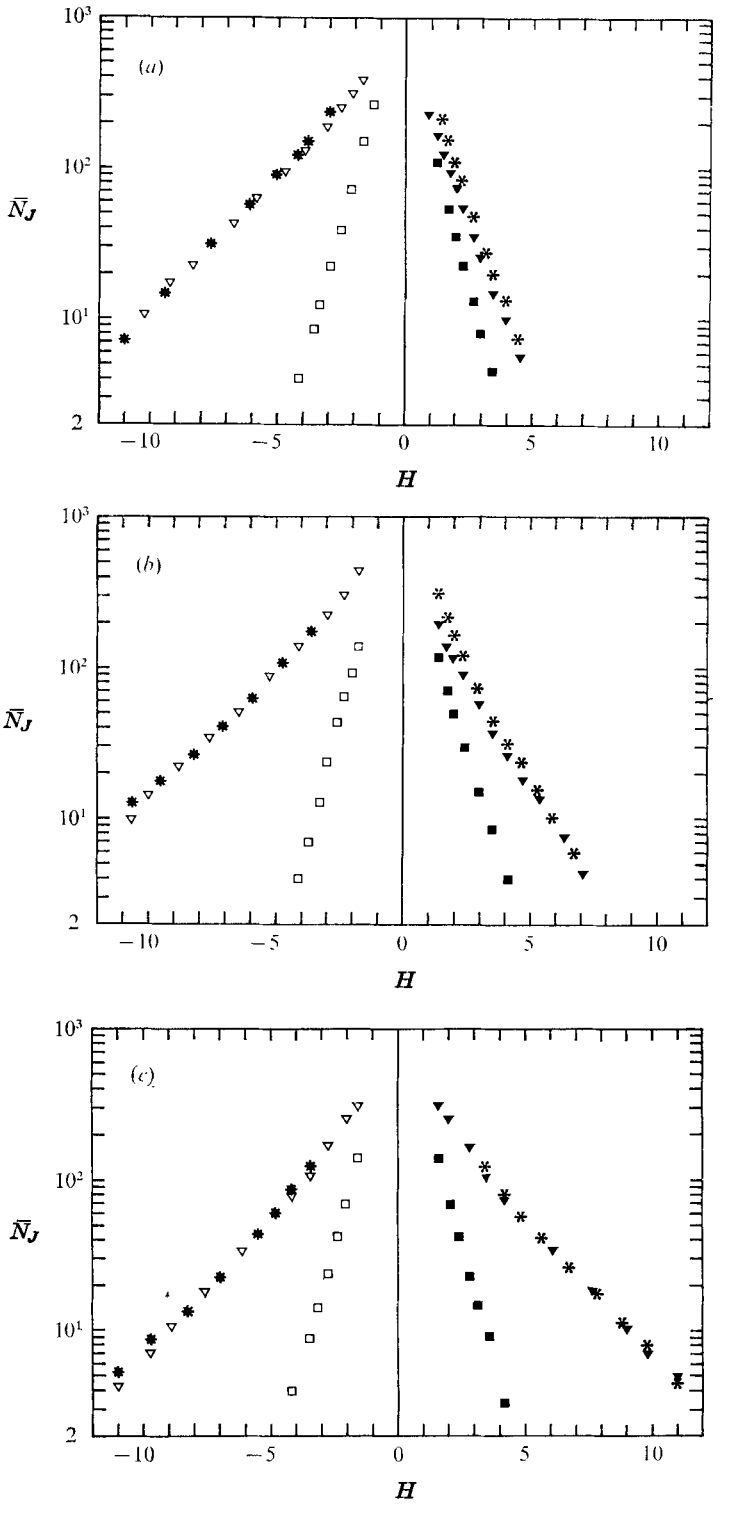

FIGURES 9(*a–c*). For legend see facing page.

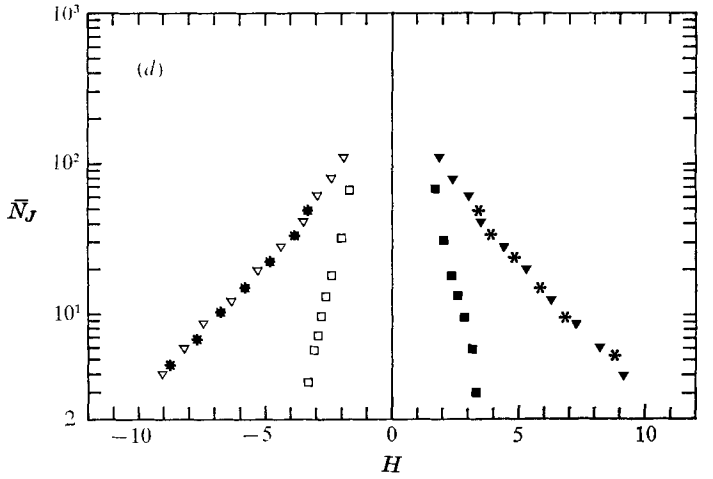

FIGURE 9. Frequency distribution of $u_1 u_2$ for the various classes of event. (*a*) Re = 135 000, x_2/R = 0·70. (*b*) Re = 135 000, x_2/R = 0·85. (*c*) Re = 135 000, x_2/R = 1. (*d*) Re = 68 000, x_2/R = 1.

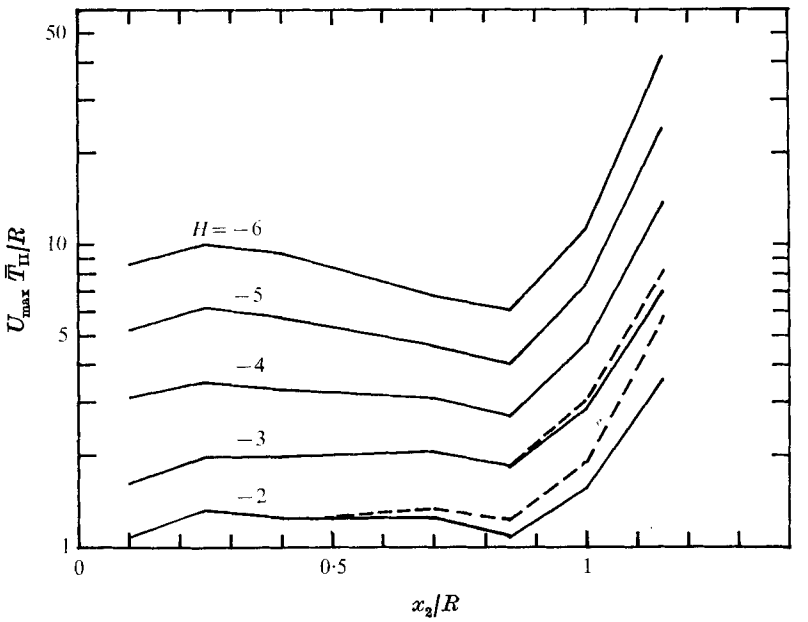

FIGURE 10. Mean time interval $\bar{T}_{II}$ between the bursts originating from a given half of the flow as function of the distance from the wall x_2/R for various values of the threshold $H = u_1 u_2/u_1' u_2'$ (Re = 135 000). – – – –, values corrected for the mean number of inward interactions related to the opposite flow (Re = 135 000).

In figure 11, all the bursts are now taken into account, irrespective of their wall origin. The values of $U_{max}\bar{T}_B/R$ are plotted *vs.* x_2/R with H as a parameter (Re = 135 000). For a given value of H, the mean time interval $\bar{T}_B$ between the bursts is deduced from the frequency $\bar{N}_B$ obtained by adding the mean frequencies of occurrence of the events of type II and III (table 2). For x_2/R = 0·85 and 1·0,

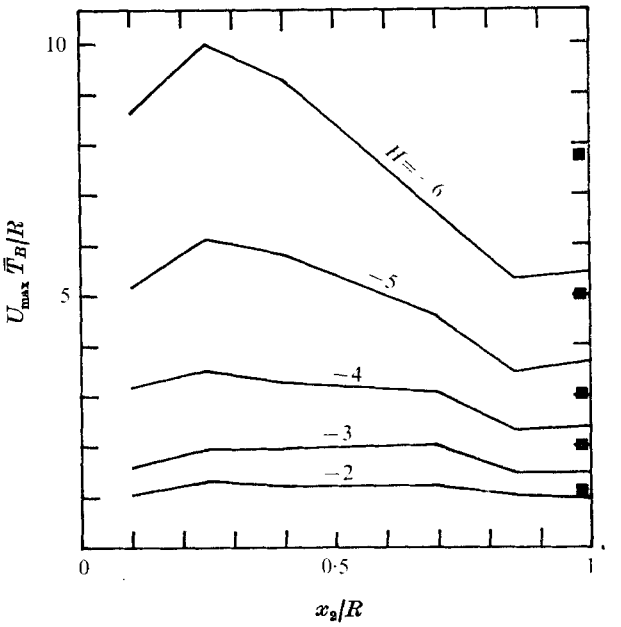

FIGURE 11. Mean time interval $\overline{T}_{II}$ between bursts (irrespective of their origin) as function of the distance from the wall x_2/R for various values of the threshold $H = u_1u_2/u_1'u_2'$. ——, Re = 135 000; ■, Re = 68 000.

and for $H = -2$ and -3, the values are corrected for the inward interactions as explained above.

The effect of the Reynolds number on the mean time interval $\overline{T}_B$ between all the bursts is considered in figure 11, in which are presented the values of $U_{max}\overline{T}_B/R$ obtained for $x_2/R = 1$ at $Re = 68\,000$. The scaling of $\overline{T}_B$ with the outer parameters of the pipe flow seems valid in the core region; however, the preferential sensitivity of the probe in this region (as explained in § 5) makes it difficult to formulate a definitive conclusion.

5. Characteristic mean time interval between bursts

The mean time $\overline{T}_{II}$ between the $[u_1u_2]_{II}$ events has been found to depend on the threshold H (§4). In order to obtain a characteristic value of $\overline{T}_{II}$ related to the most violent bursts, it is therefore necessary to find a relevant threshold. A satisfactory criterion has been suggested by Lu & Willmarth (1973). It is based on an analysis of the fractional contribution from every quadrant J to the local mean Reynolds stress $\overline{u_1u_2}$. The relevant threshold, denoted by H_c, is such that only the bursts related to a given half of the flow contribute to the local mean value $\overline{u_1u_2}$ of the Reynolds shear stress fluctuation (the corresponding sweeps and interactions having a negligible contribution at this threshold). In figure 12 are shown the fractional contributions $\overline{[u_1u]_J}/\overline{u_1u_2}$ for J = I, II, III, IV at different distances from the wall: $x_2/R = 0{\cdot}10$, $0{\cdot}25$, $0{\cdot}40$, $0{\cdot}70$, $0{\cdot}85$ for $Re = 135\,000$, and $x_2/R = 0{\cdot}25$ for $Re = 68\,000$.

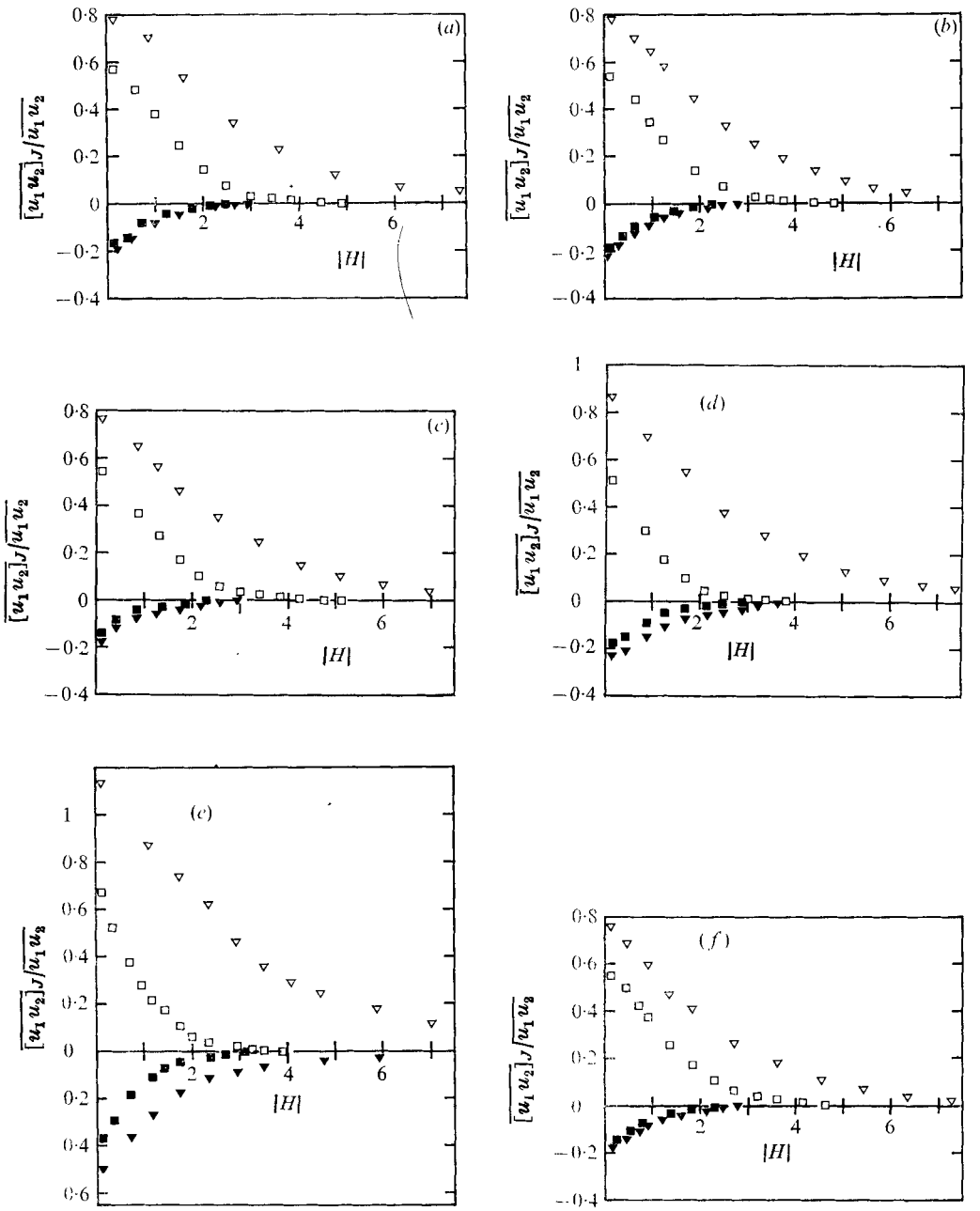

FIGURE 12. Contribution to $\overline{u_1 u_2}$ from the different classes of event. ■, $[u_1 u_2]_{\mathrm{I}}$; ▽, $[u_1 u_2]_{\mathrm{II}}$; ▼, $[u_1 u_2]_{\mathrm{III}}$; □, $[u_1 u_2]_{\mathrm{IV}}$. (*a*) $Re = 135\,000$, $x_2/R = 0{\cdot}10$. (*b*) $Re = 135\,000$, $x_2/R = 0{\cdot}25$. (*c*) $Re = 135\,000$, $x_2/R = 0{\cdot}40$. (*d*) $Re = 135\,000$, $x_2/R = 0{\cdot}70$. (*e*) $Re = 135\,000$, $x_2/R = 0{\cdot}85$. (*f*) $Re = 68\,000$, $x_2/R = 0{\cdot}85$.

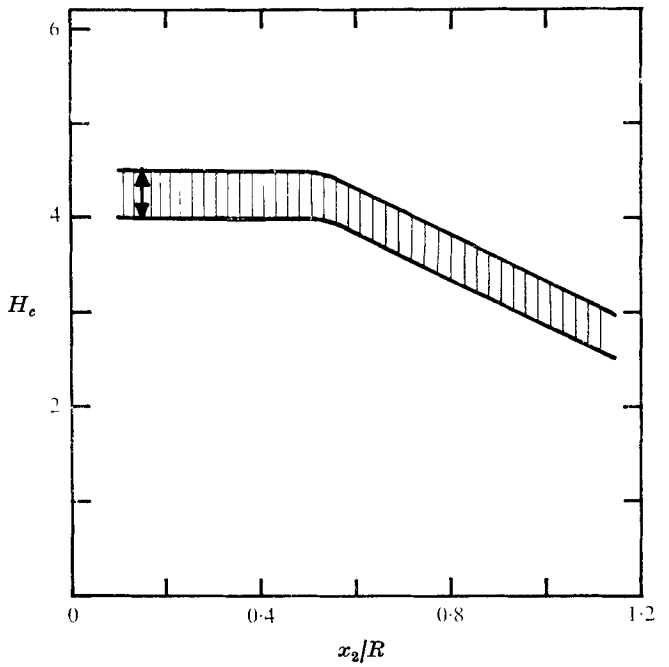

FIGURE 13. Characteristic value H_c of the threshold as a function of the distance from the wall x_2/R (Re = 135 000).

The results obtained in the 'inner' region (i.e. at x_2/R = 0·10, 0·25, 0·40) are in very good agreement with the earlier results obtained by Lu & Willmarth (1973) in a boundary layer. The bursts give the dominant contributions to the mean Reynolds stress (approximately 80 % for $H = 0$) and the characteristic threshold H_c is located between -4 and $-4{\cdot}5$.

In the core region, the results contrast with those obtained in a boundary layer: H_c decreases towards the pipe axis (figure 13). This behaviour can be explained by the focusing effect caused by the geometry of the wall, and the preferential sensitivity of an X-probe. In fact, ejections in a pipe flow can occur along any azimuthal direction (i.e. along any radius), but an X-probe located on the Ox_2 axis has an optimal u_2 sensitivity for motions occurring precisely along Ox_2 (figure 14). If an ejection occurs along a direction Δ different from Ox_2, the signal transmitted and consequently the u_1u_2 product obtained are reduced. In order to take into account all the 'equivalent' bursts occurring from any direction, the characteristic threshold H_c must therefore appear in the core region at a smaller value than in the wall region, where all the ejections detected by the probe occur near Ox_2. We can expect that in a channel flow this effect would not be observed and that the characteristic threshold H_c would be nearly constant throughout the flow as in boundary layers.

The characteristic mean time interval $\overline{T}_{c,\,\mathrm{II}}$ between the bursts related to a given half of the pipe circumference has been deduced from the above values of H_c, by $\overline{T}_{c,\,\mathrm{II}} \equiv 1/\overline{N}_{c,\,\mathrm{II}} \equiv 1/f_{\mathrm{II}}(H_c)$. The results are given in figure 15. The focusing effect seems to be largest in the neighbourhood of x_2/R = 0·85, where the number

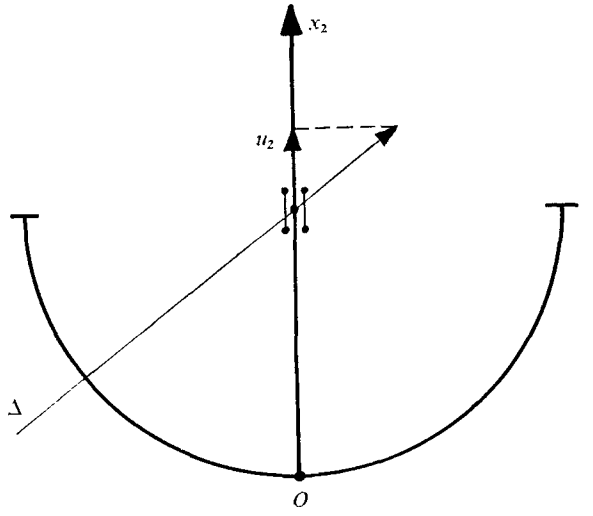

FIGURE 14. Sketch showing the directional sensitivity of an X-probe (effect related to the u_2 signal).

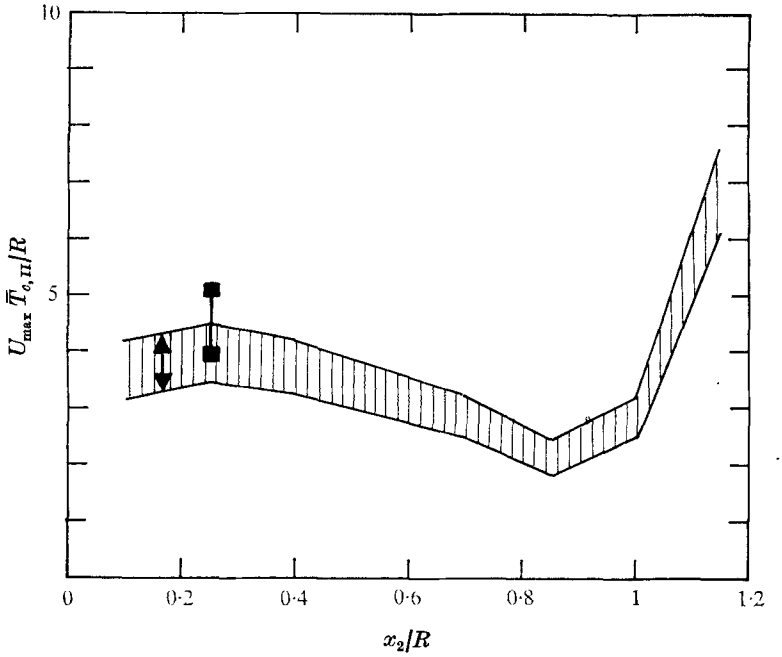

FIGURE 15. Characteristic mean time interval $\overline{T}_{c,II}$ between the violent bursts originating from a given half of the flow as a function of the distance from the wall x_2/R. ——, Re = 135 000; ■, Re = 68 000.

of bursts per unit time is found to be approximately twice as great as in the wall region.

In figure 16, all the bursts have been taken into account irrespective of their origin (i.e. from opposite halves of the flow) in order to define a characteristic mean time interval $\overline{T}_{c,B}$ between all the bursts. In the inner part of the flow, the

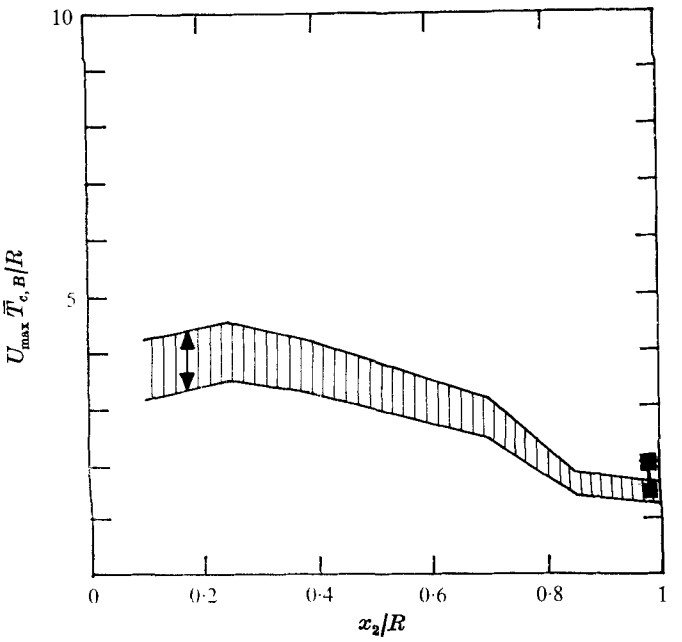

FIGURE 16. Characteristic mean time interval $\bar{T}_{c,B}$ between the violent bursts (irrespective of their origin) as function of the distance from the wall x_2/R. ——, Re = 135 000; ■, Re = 68 000.

results are again in agreement with those of Lu & Willmarth (1973), obtained in a boundary layer. In the core region of the pipe, however, the number of bursts per unit time is roughly three times higher than in the wall region. Furthermore, this ratio is certainly still too small because the X-probe does not detect the bursts occurring along a direction nearly normal to Ox_2 (figure 14).

6. Mean duration of bursts

The intermittency of the Reynolds shear stress fluctuation is mainly associated with the burst events, and so the value of the characteristic mean time interval between the bursts provides a first property of this intermittent phenomenon. A second property is related to the mean duration of the bursts. In preliminary experiments, the mean duration $\overline{\Delta T}_{II}$ of the $[u_1 u_2]_{II}$ events was obtained by measuring the mean time during which the corresponding signal exceeded the threshold H_c. The experiments were conducted by means of a periodic pulse train of 100 kHz which was substituted for the 3 V d.c. voltage at the second analog gate (figure 4). The mean duration $\overline{\Delta T}_{II}$ was then deduced from the number of pulses counted per unit time at the gate output and from the mean frequency $\bar{N}_{II}$ of the bursts events. Figure 17 shows the variation of the mean duration $\overline{\Delta T}_{II}$ across the flow for various values of H ($H = -2{\cdot}5,\ -3{\cdot}5,\ -4{\cdot}5,\ -5$) and for Re = 135 000. Compared with the mean frequency $\bar{N}_{II}$ of the burst events (see figure 10), it is observed that $\overline{\Delta T}_{II}$ depends less on the threshold H than the mean frequency $\bar{N}_{II}$. For instance, at $x_2/R = 0{\cdot}25$, when H varies from 2·5 to 5, $\overline{\Delta T}_{II}$

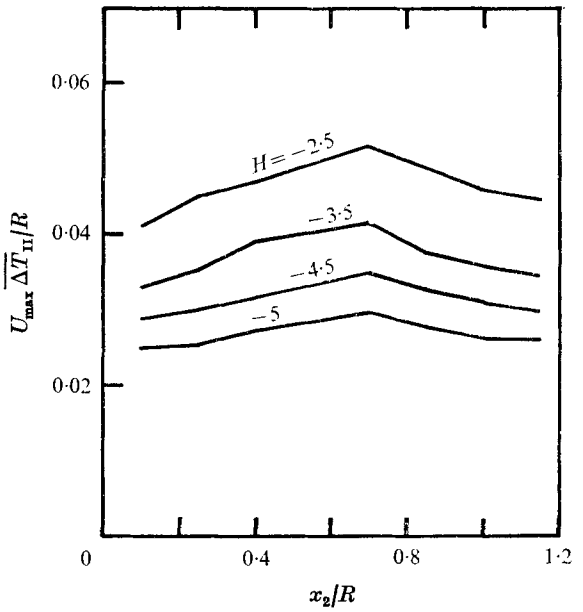

FIGURE 17. Mean duration $\overline{\Delta T}_{II}$ of bursts originating from a given half of the flow as a function of the distance from the wall x_2/R for various values of the threshold $H = u_1 u_2/u_1' u_2'$. (Re = 135 000.)

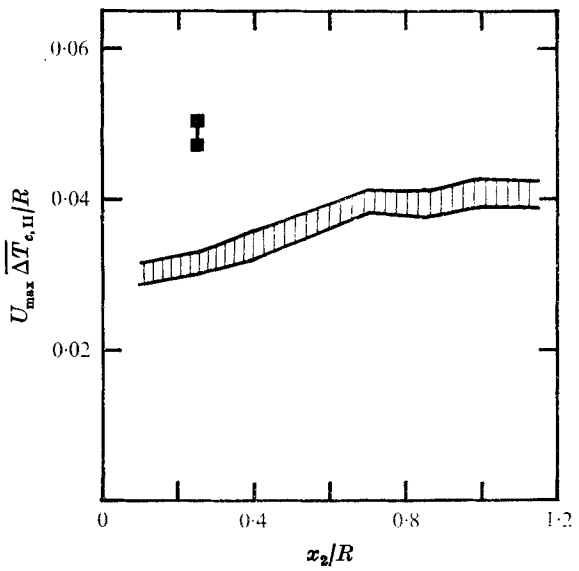

FIGURE 18. Characteristic mean duration $\Delta T_{c,II}$ of the violent bursts originating from a given half of the flow as a function of the distance from the wall x_2/R. ——, Re = 135000; ■, Re = 68000.

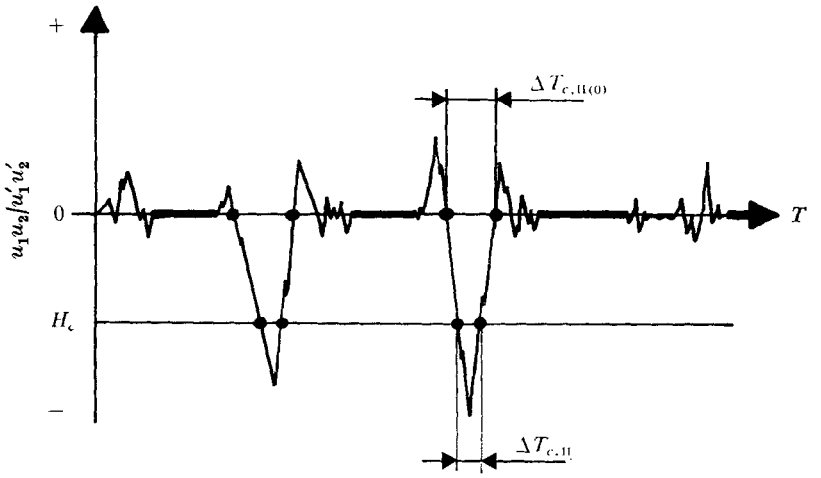

FIGURE 19. Sketch showing the incremental durations $\Delta T_{c,\mathrm{II}}$ and $\Delta T_{c,\mathrm{II}(0)}$ used in the definition of the characteristic mean durations $\overline{\Delta T}_{c,\mathrm{II}}$ and $\overline{\Delta T}_{c,\mathrm{II}(0)}$ of the violent bursts.

decreases by a factor of about 2·5, whereas $\bar{N}_{\mathrm{II}}$ decreases by a factor of about 4. This result confirms that for the large 'pulses' of $[u_1u_2]_{\mathrm{II}}$ the time derivative $\partial[u_1u_2]/\partial t$ is very high, so that the duration of bursts is short (see figure 2). A characteristic mean duration $\overline{\Delta T}_{c,\mathrm{II}}$ of bursts can be simply defined as the mean duration of bursts for which the $[u_1u_2]_{\mathrm{II}}$ signal exceeds the specific level H_c obtained previously (§5). Figure 18 shows the variation of $\overline{\Delta T}_{c,\mathrm{II}}$ across the flow for $Re = 135\,000$. The outer parameters $U_{\max}$ and R have been used to make $\overline{\Delta T}_{c,\mathrm{II}}$ dimensionless. The value of $\overline{\Delta T}_{c,\mathrm{II}}U_{\max}/R$ obtained at $x_2/R = 0{\cdot}25$ for $Re = 68\,000$ is also plotted in figure 18. Compared with the corresponding results obtained at $Re = 135\,000$ and with the earlier results obtained by Lu & Willmarth in a boundary layer at $Re_\delta \simeq 50\,000$ and $Re_\delta \simeq 500\,000$, we conclude that scaling the mean duration of bursts with the outer parameters of the flow is not appropriate.

In order to define the length scale of bursts, the above definition of $\overline{\Delta T}_{c,\mathrm{II}}$ is not fully satisfactory since the duration of the most 'violent' bursts is taken at the level H_c although those bursts exist at lower amplitudes of u_1u_2 (figure 19). It is the 'base' of the burst which has a physical meaning and a knowledge of the corresponding mean duration $\overline{\Delta T}_{c,\mathrm{II}(0)}$ is required. This duration is not, however, directly obtainable since for $H = 0$ all the bursts are taken into account and not only the most violent bursts. The indirect approach which has been used consists of an extrapolation towards $H = 0$ of the function $\overline{\Delta T}_{\mathrm{II}} = g(H)$ defined from the large values of $|H|$ (i.e. $3 \lesssim |H| \lesssim 7$). Such an extrapolation shows that the characteristic mean duration $\overline{\Delta T}_{c,\mathrm{II}(0)}$ is roughly twice as large as the mean duration $\overline{\Delta T}_{c,\mathrm{II}}$ defined for $H = H_c$. These values of $\overline{\Delta T}_{c,\mathrm{II}(0)}$ can be used to estimate a characteristic mean longitudinal length scale l of bursts by means of the Taylor hypothesis: $l = U\overline{\Delta T}_{c,\mathrm{II}(0)}$. The values of l obtained across the flow are given in table 1, where the longitudinal integral length scales $L_{22}^{(1)}$ and $L_{22}^{(1)}$ obtained earlier (Sabot & Comte-Bellot 1972*a*, *b*, 1974) are also recorded. It appears that l is of

the same order of magnitude as the longitudinal integral length scale $L_{22}^{(1)}$ associated with the radial velocity component u_2 and noticeably lower than the longitudinal integral length scale $L_{11}^{(1)}$ associated with the longitudinal velocity component u_1. This result strongly suggests that the space coherency of u_2 is mainly related to the burst-like motions and that the space coherency of u_1 is presumably related to other larger-scale motions. The present experiments provide no information about the lifetime of the bursts. However, an order of magnitude can be provided by the value of the integral time scale $\Theta_{22}^{(1)}$ deduced from the optimal time autocorrelation of u_2 in a convected frame (Sabot, Renault & Comte-Bellot 1973; Sabot & Comte-Bellot 1974) if the time coherency of the radial velocity component u_2 is assumed to be mainly associated with the burst-like motions. Values of $\Theta_{22}^{(1)}$ across the flow are given in table 1 as well as the values of $\Theta_{11}^{(1)}$, which are noticeably larger than $\Theta_{22}^{(1)}$.

7. Space–time correlations measurements

In the present work, the space–time correlations which are investigated are those which could provide data on the possible existence, in the pipe core region, of large-scale rotating structures similar to those observed in the outer part of boundary layers (Kovasznay *et al.* 1970; Nychas *et al.* 1973). In these measurements, the hot-wire equipment was the same as previously. The time correlations were obtained by a real-time correlator (Soc. Appl. In. Phys. type CTR 100, or Hewlett–Packard model 3721 A). The frequency bandwidth was in the range 4 Hz–20 kHz.

The first set of measurements deals with the space–time correlation coefficient of the radial velocity component,

$$R_{22}(\mathbf{x}; r_1, 0, 0; \tau) \equiv \frac{\overline{u_2(x_1, x_2, x_3; t)\, u_2(x_1 + r_1, x_2, x_3; t + \tau)}}{u_2'(x_1, x_2, x_3)\, u_2'(x_1 + r_1, x_2, x_3)},$$

and the results obtained at two distances from the wall, $x_2/R = 1{\cdot}0$ and $0{\cdot}50$, are given in figures 20 (*a*) and (*b*). Negative lobes appear in the curves which concern the core region, at time delays smaller than the optimum delay τ_m. At large r_1 separations, only an antisymmetrical pattern remains. Kovasznay *et al.* (1970) observed a similar sort of behaviour in the outer part of a boundary layer where a forward rotational motion in the bulges had been inferred from conditionally sampled measurements. These authors have also explained why the antisymmetrical pattern of $R_{22}(\mathbf{x}; r_1, 0, 0; \tau)$ is associated with a forward rotational motion inside the bulge. If such a description is extended, in the core region of the pipe, to bulges originating from opposite halves of the flow, then the same shape of curve $R_{22}(\mathbf{x}; r_1, 0, 0; \tau)$ is obtained for each kind of bulge. It is therefore not surprising that the measured correlations, which are weighing motions from both sides, keep the same antisymmetric pattern as in the outer part of a boundary layer. Besides, no negative lobes have been observed on the curves $R_{11}(\mathbf{x}; r_1, 0, 0; \tau)$ concerning the longitudinal fluctuation u_1 at $x_2/R = 1$ (Sabot & Comte-Bellot 1971), a result again analogous to that obtained in the outer part of a boundary layer by Kovasznay *et al.* (1970).

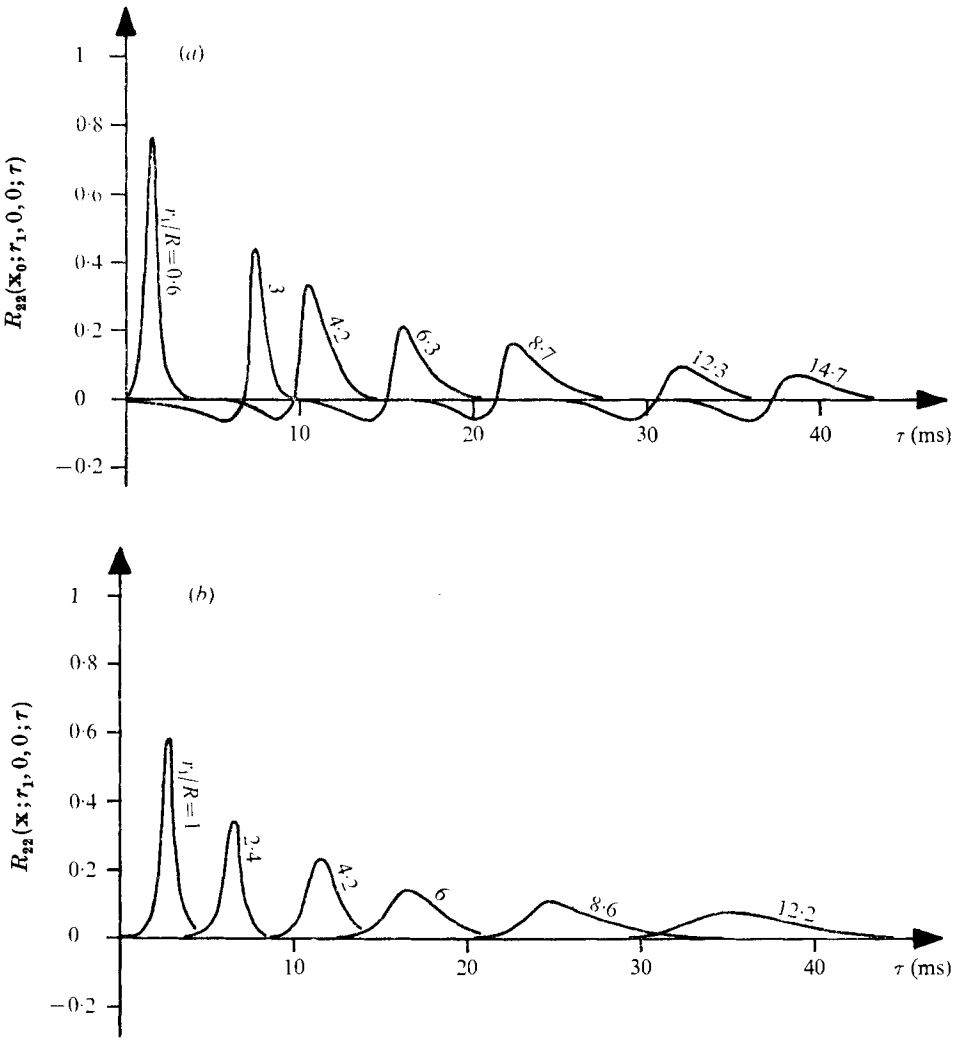

FIGURE 20. Space–time correlation functions $R_{22}(\mathbf{x}; r_1, 0, 0; \tau)$ of the radial velocity fluctuation u_2 for (*a*) $x_2/R = 1$ and (*b*) $x_2/R = 0{\cdot}50$ ($Re = 135\,000$).

The second set of results deals with the space–time correlation coefficients $R_{12}(\mathbf{x}; 0, r_2, 0; \tau)$, for which the fixed probe is located on the pipe axis and provides the longitudinal velocity fluctuations u_1, whereas the moveable probe, which provides the radial velocity fluctuation u_2, is located in the same section as the fixed probe at various radial separations r_2. An antisymmetric pattern is observed on the curves $R_{12}(\mathbf{x}; 0, r_2, 0; \tau)$ until $r_2/R \simeq 0{\cdot}35$ (figure 21) with negative lobes for negative time delays. This behaviour is again consistent with a possible forward rotational motion inside the bulges in the core region (as sketched in figure 22). From the time increment $\Delta\tau$ over which the antisymmetrical pattern of $R_{12}(\mathbf{x}; 0, r_2, 0; \tau)$ occurs it is possible to obtain, with the help of the Taylor hypothesis, a rough estimate of the mean longitudinal extent $\mathscr{L}$ of the possible

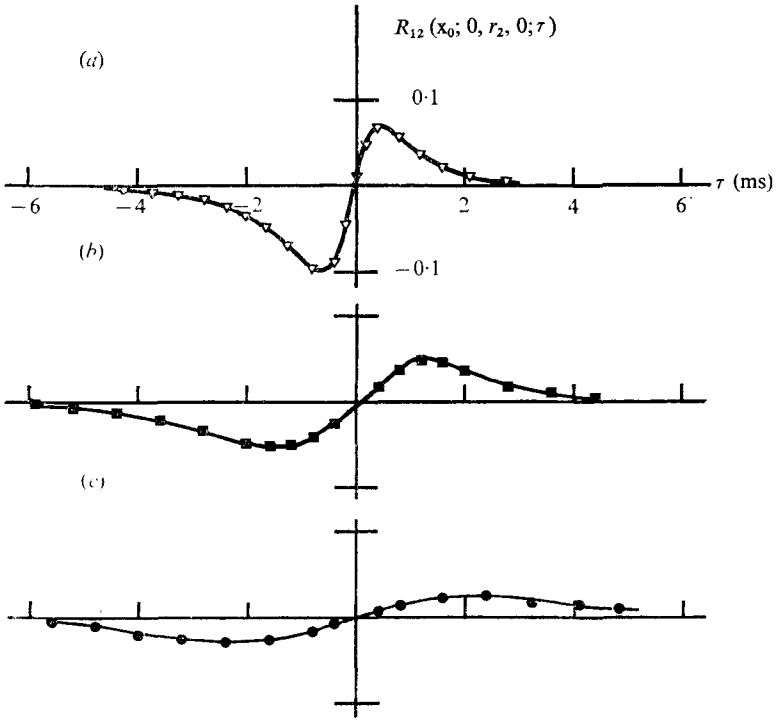

FIGURE 21. Space–time correlation functions $R_{12}(\mathbf{x}; 0, r_2, 0; \tau)$ of the streamwise and radial velocity fluctuations. The first probe is fixed on the axis and provides $u_1(t)$. The second probe may be moved along a radius and provides the delayed signal $u_2(t+\tau)$. ($Re = 68\,000$.) (*a*) $r_2/R = 0{\cdot}10$. (*b*) $r_2/R = 0{\cdot}25$. (*c*) $r_2/R = 0{\cdot}35$.

large-scale rotating motions. If, as a lower value, the time interval $\Delta\tau$ between the positive and negative extrema on the curve $R_{12}(\mathbf{x}; 0, r_2, 0; \tau)$ corresponding to the intermediate radial separation $r_2/R = 0{\cdot}25$ of the probes is retained, then figure 21 provides $\Delta\tau \simeq 3$ ms, so that $\mathscr{L}/R \simeq 0{\cdot}6$. This value is not very different from that directly observed in boundary layers for $x_2/\delta = 1$ and for Reynolds numbers of the same order of magnitude as that now investigated (Kovasznay *et al.* 1970; Antonia 1972). In addition, this value appears to be noticeably larger than the value l/R previously deduced from the characteristic mean duration $\overline{\Delta T}_{c,\,\mathrm{II}\,(0)}$ of bursts since the ratio $\mathscr{L}/l$ is of the order of 6.

8. Conclusions

The structure of the instantaneous Reynolds shear stress sorted into the four quadrants of the u_1, u_2 plane across a fully developed turbulent pipe flow has been investigated. It exhibits two distinct properties according to the region of the flow considered.

In the 'inner' part of the flow, defined as the wall side of the core region, where the correlation coefficient $\overline{u_1 u_2}/u_1' u_2'$ does not change appreciably with x_2/R, the structure of the Reynolds stress is dominated by the bursts, i.e. by ejection of low speed fluid towards the pipe axis, and the main properties observed are as follows.

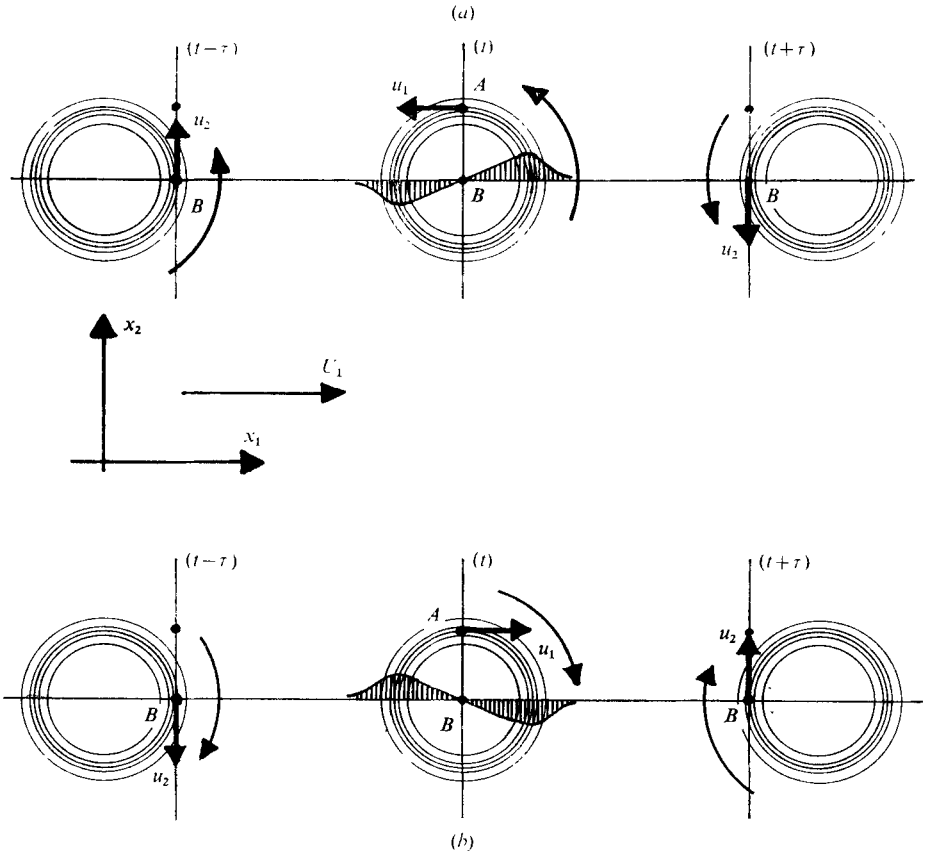

FIGURE 22. Sketches showing the velocity components u_1 and u_2 induced by a forward rotational motion inside the convected bulges at points $A(\mathbf{x})$ and $B(\mathbf{x};\ 0,\ r_2,\ 0)$ and at the three instants $t-\tau$, t, $t+\tau$. (*a*) Bulges related to wall 1. (*b*) Bulges related to wall 2. For either case $u_1^A(t)u_2^B(t-\tau) < 0$ and $u_1^A(t)u_2^B(t+\tau) > 0$.

(i) The characteristic mean time interval $\overline{T}_{c,\,\mathrm{II}}$ between bursts defined as in Lu & Willmarth's (1973) experiments does not vary appreciably with x_2/R.

(ii) The scaling of the characteristic mean time interval $\overline{T}_{c,\,\mathrm{II}}$ with the outer parameters of the flow is checked since $U_{\max}\overline{T}_{c,\,\mathrm{II}}/R \simeq U_\infty \overline{T}_{c,\,\mathrm{II}}/\delta \simeq -4$ for Reynolds numbers between approximately 50 000 and 500 000 (when using the present data and the earlier data of Lu & Willmarth 1973).

(iii) The regions of violent stress form a small percentage of the overall region of the flow (5–10 %).

(iv) The mean duration of the bursts suggests that the integral length scale $L_{22}^{(1)}$ of the radial velocity component u_2 is mainly associated with the burst-like motions.

(v) Scaling the mean duration of the bursts with the outer parameters is not appropriate.

In the core region of the pipe flow, the variation of the correlation coefficient $\overline{u_1 u_2}/u_1' u_2'$ with x_2/R is due to a new structure of the Reynolds stress, characterized by the following properties.

(i) Large negative values of $u_1 u_2$ are still observed and associated with ejections of low speed fluid, i.e. bursts, related to a given half of the flow, but in addition, very large positive values of $u_1 u_2$ are also observed. These new events are associated with ejections of low speed fluid originating from the opposite half of the flow. Two distinct burst-like patterns exist therefore in the core region. In particular, on the pipe axis, the zero value of $\overline{u_1 u_2}$ is due to the symmetry of the flow and does not result from an isotropic state of the turbulence in the core region.

(ii) For a given burst-like pattern, i.e. the pattern related to a given half of the flow and for which $u_1 < 0$ and $u_2 > 0$, the characteristic mean time interval $\overline{T}_{c,\,\mathrm{II}}$ between the bursts depends on the distance from the wall x_2/R.

(iii) A focusing effect caused by the circular geometry of the wall (i.e. related to ejections occurring in any azimuthal direction) is observed. It is largest near $x_2/R = 0{\cdot}85$, where the characteristic mean number of bursts is approximately twice that in the wall region.

(iv) The most violent bursts related to a given half of the flow penetrate into the other half of the flow up to about $x_2/R = 1{\cdot}3$.

(v) When all the bursts are taken into account (i.e. those originating from the opposite halves of the flow) their total number has a maximum on the pipe axis and is roughly 3 times higher than in the wall region. Furthermore, this value must be considered as a minimum estimate because ejections occurring along a direction nearly normal to Ox_2 are not detected by an X-probe.

(vi) Specific space–time velocity correlations $R_{22}(r_1, 0, 0; \tau)$ and $R_{12}(0, r_2, 0; \tau)$ exhibit characteristic antisymmetrical patterns in the core region when plotted *vs.* the time delay τ. This behaviour provides new evidence of the possible existence of rotating structures similar to those observed earlier in the outer part of a turbulent boundary layer (Kovasznay *et al.* 1970; Nychas *et al.* 1973). These coherent motions are found to have a scale noticeably larger than that of the bursts.

Part of this work was presented at the Colloquium on Coherent Structures in Turbulence, held at the University of Southampton, in March 1974. The authors are very indebted to Professor J. L. Lumley and Dr F. P. Ricou for helpful conversations during the editing of the article and to referee B for noticing an error in measurements dealing with the mean duration of bursts.

REFERENCES

Antonia, R. A. 1972 *J. Fluid Mech.* **56**, 1.

Bradshaw, P., Dean, R. B. & McEligot, D. M. 1973 *J. Fluids Engng, Trans. A.S.M.E.* I **40**, 214.

Brodkey, R. S., Wallace, J. M. & Eckelmann, H. 1974 *J. Fluid Mech.* **63**, 209.

Comte-Bellot, G. 1965 *Publ. Sci. Tech. du Ministère de l'Air, Paris*, no. 419. (Trans. P. Bradshaw 1969 *Aero. Res. Counc. R. & M.* no. 31, 609.)

Comte-Bellot, G. & Marechal, J. 1963 *Intern. Rep., Université de Grenoble.*

Corino, E. R. & Brodkey, R. S. 1969 *J. Fluid Mech.* **37**, 1.

Corrsin, S. & Kistler, A. L. 1955 *N.A.C.A. Rep.* no. 1244.

FALCO, R. E. 1974 *A.I.A.A. 12th Aerospace Sci. Meeting, Washington*, paper 74-99.

GRASS, A. J. 1971 *J. Fluid Mech.* **50**, 233.

KIM, H. T., KLINE, S. J. & REYNOLDS, W. C. 1971 *J. Fluid Mech.* **50**, 133.

KLINE, S. J., REYNOLDS, W. C., SCHRAUB, F. A. & RUNSTADLER, P. W. 1967 *J. Fluid Mech.* **30**, 741.

KOVASZNAY, L. S. G., KIBENS, V. & BLACKWELDER, R. F. 1970 *J. Fluid Mech.* **41**, 283.

LAUFER, J. & BADRI NARAYANAN, M. A. 1971 *Phys. Fluids*, **14**, 182.

LU, S. S. & WILLMARTH, W. W. 1973 *J. Fluid Mech.* **60**, 481.

NYCHAS, S. G., HERSHEY, H. C. & BRODKEY, R. S. 1973 *J. Fluid Mech.* **61**, 513.

PATEL, V. C. 1974 *Aero. J.* **78**, 93.

PERRY, A. E. & ABELL, C. J. 1975 *J. Fluid Mech.* **67**, 257.

RAO, K. N., NARASIMHA, R. & BADRI NARAYANAN, M. A. 1971 *J. Fluid Mech.* **48**, 339.

SABOT, J. & COMTE-BELLOT, G. 1971 *C.r. Acad. Sci. Paris*, A **273**, 638.

SABOT, J. & COMTE-BELLOT, G. 1972*a* *C.r. Acad. Sci. Paris*, A **275**, 1647.

SABOT, J. & COMTE-BELLOT, G. 1972*b* *C.r. Acad. Sci. Paris*, A **275**, 667.

SABOT, J. & COMTE-BELLOT, G. 1974 *C.r. Acad. Sci. Paris*, A **278**, 105.

SABOT, J., RENAULT, J. & COMTE-BELLOT, G. 1973 *Phys. Fluids*, **16**, 1403.

WALLACE, J. M., ECKELMANN, H. & BRODKEY, R. S. 1972 *J. Fluid Mech.* **54**, 39.

WILLMARTH, W. W. & LU, S. S. 1972 *J. Fluid Mech.* **55**, 65.